THESIS FOR THE DEGREE OF DOCTOR OF PHILOSOPHY IN SOLID AND STRUCTURAL MECHANICS

Machine Tool Dynamics

A constrained state-space substructuring approach

ANDERS LILJEREHN

Department of Applied Mechanics
CHALMERS UNIVERSITY OF TECHNOLOGY
Göteborg, Sweden 2016

Machine Tool Dynamics
A constrained state-space substructuring approach
ANDERS LILJEREHN
ISBN 978-91-7597-507-8

© ANDERS LILJEREHN, 2016

Doktorsavhandlingar vid Chalmers tekniska högskola
Ny serie nr. 4188
ISSN 0346-718X
Department of Applied Mechanics
Chalmers University of Technology
SE-412 96 Göteborg
Sweden
Telephone: +46 (0)31-772 1000

Cover:
Exemplified substructure partition strategy using a mixture of experimental and analytical model descriptions

Chalmers Reproservice
Göteborg, Sweden 2016

Machine Tool Dynamics - A constrained state-space substructuring approach

Anders Liljerehn
Division of Dynamics
Department of Applied Mechanics
Chalmers University of Technology

Abstract

Metal cutting is today one of the leading forming processes in the manufacturing industry. The metal cutting industry houses several actors providing machine tools and cutting tools with a fierce competition as a consequence. Extensive efforts are made to improve the performance of both machine tools and cutting tools. Performance improvements are not solely restricted to produce stronger and more durable machine tools and cutting tools. They also include knowledge about how the machine tools and cutting tools should be used to perform at an optimum of their combined capacity. Information about the dynamic properties of the machine tool cutting tool assembly is one of the aspects that carries the most potential in terms of productivity increase and process reliability. This work presents a methodology to synthesise the dynamic behaviour of a machine tool and cutting tool assembly based on component models of the machine tool and the cutting tool. The system is treated as an assembly of subcomponents in order to reduce measurement effort. The target is to get the receptance at the tip of the machine tool/cutting tool which is a prerequisite for process analysis and optimisation. This methodology is compared with today's state-of-the-art methodology which require experimental testing for each cutting tool of interests mounted in the machine tool. Comparisons are also made with previous attempts to utilize component synthesis in this matter. The subcomponent approach presented here limits the experimental tests to the machine tool component. The machine tool component model is connected to a model representation, based on a finite element model of the cutting tool. The subcomponent models are obtained and coupled on state-space form, a technique that is new to the application of component synthesis of machine tool/cutting tool structures. Proposed procedures for measurements, system identification, enforcement of physical properties on state-space models and parameter influences on coupled results are presented, implemented and validated. This methodology opens windows not only to cutting process optimisation of an existing cutting tool but it also permits tailored cutting tool solutions for existing machining operations with fixed process parameters.

Keywords: Metal cutting, State-space component synthesis, Chatter stability, Receptance coupling, System identification, State-space models

To my loving family:
Helena, Stina and Ludvig

PREFACE

This thesis is the result of the work conducted during 2009-2016 within the project *Using predictions to avoid chatter in cutting operations* at the Department of Applied Mechanics, Division of Dynamics at Chalmers University of Technology. The project is financed by Sandvik Coromant and the Centre for Advanced Production Engineering (CAPE). The completion of this thesis owes to the following persons: My supervisor Professor Thomas Abrahamsson with his expertises within my research field and his ability to guide me in the right direction. He who always saw the positive side of my problems and always cheered me up when everything seemed hopeless. Mikael Lundblad, without whom I probably never would have had the opportunity to conduct this research. To my wife Helena without whom this project would never been completed. For her patience, support and love. To my children Stina and Ludvig for greeting me with their smiles when I come home from my work and my travels and always keeping me grounded. To Per Sjövall who helped me with and allowed me to use his state-space coupling routines. To Ronnie Hedström for allowing me to conduct experimental investigations in his fully booked machine tool on short notice. To Anders T. Johansson and Martin Magnevall for their help and support during this work and finally to Jon Nödtveidt for accompanying me during my travels to Gothenburg from Sandviken.

THESIS CONTENT

This thesis consists of an introduction and is based on the following appended papers:

Paper A A. Liljerehn, A. T. Johansson, T. Abrahamsson, Dynamic substructuring in metal cutting machine chatter. Presented at *ISMA 2010 Conference on Noise and Vibration*

Paper B A. Liljerehn, T. Abrahamsson, Experimental−Analytical Substructure Model Sensitivity Analysis for Cutting Machine Chatter Prediction. Presented at the *30th International Modal Analysis Conference 2012*

Paper C A. Liljerehn, T. Abrahamsson, Dynamic sub-structuring with passive state-space components. Presented at *ISMA 2014 Conference on Noise and Vibration*

Paper D A. Liljerehn, T. Abrahamsson, Residual compensation in experimental state space model synthesis, *Submitted for International Journal Publication*, 2016

Paper E A. Liljerehn, T. Abrahamsson, On rotational degrees of freedom for substructure synthesis of machine tool and cutting tools, *In manuscript*, 2016

The appended papers were prepared in collaboration with co-authors. The author of this thesis was responsible for the major progress of work, including taking part in planning the papers, developing the theory, developing and carrying out measurements, the numerical implementations and writing the reports.

Contents

Abstract **i**

Preface **v**

Thesis content **vii**

Contents **x**

I Extended summary **1**

1 Introduction and motivation **1**
1.1 Aim and scope 4

2 Models in structural dynamics **4**
2.1 Time domain modeling 4
2.2 Frequency domain modeling 6
2.3 System identification 7

3 Component synthesis theory **9**
3.1 Component mode synthesis, CMS 10
3.2 Frequency based substructuring, FBS 10
3.2.1 Impedance coupling method 10
3.2.2 Generalised FRF impedance coupling technique 12
3.3 State-space based coupling 13

4 Machining dynamics by component synthesis **14**
4.1 Cutting tool model 16
4.2 Substructure partition 17
4.2.1 Machine tool/tool holder partition 19
4.2.2 Integrated cutting tool partition 22

5 Motivation to the state-space approach **25**
5.1 Noise free data 25
5.2 Rotational degrees of freedom, RDOF 25

6 Experimental uncertainties **27**
6.1 Test results inconsistent with principles of physics 27
6.1.1 Truncation effects 29
6.2 Physical model consistency 32
6.3 Linear time-invariant systems 33

7 Chatter vibrations in metal cutting **36**
7.1 Chatter in turning of a disk 36
7.1.1 Stability lobe diagrams in turning 37
7.2 Chatter in milling 39
7.2.1 Stability lobe diagrams in milling 40
7.3 Time domain chatter stability boundary 44

8 Summary of appended papers **46**

9 Conclusions and future work **48**

References **48**

II Appended papers A-E

Paper A **A1-A17**

Paper B **B1-B18**

Paper C **C1-C14**

Paper D **D1-D27**

Paper E **E1-E30**

Part I

Extended summary

The purpose of the extended summary is to provide a background and further insight to the theoretical framework that this work relies upon. Some of the theories presented in this section have been utilized in the result evaluation reported in the presented papers yet only acknowledged by citations. Hence to further facilitate the reader, a more extensive theoretical and philosophical background is provided here along with references to the appended papers where appropriate.

1 Introduction and motivation

The strong competition in manufacturing industry has lead to a constant search for efficient cutting operations to reduce cost. Increased productivity require faster machining and lower cycle times. In order to meet these demands it is desired that process parameters, such as cutting speed, feed velocity and depth of cut are increased. As a consequence of these process parameter modifications, an increase in cutting forces and temperature in the cutting zone follows. Elevated thermal and mechanical loads accelerates tool wear and may contribute to form errors and increases the surface roughness of the work piece. Further it may drive the cutting process to an unstable regime where the vibration levels for some time grow exponentially which can causes severe damage to the cutting tool, work piece and machine tool.

The ability to model the dynamic response at the tip of the machine tool mounted cutting tool is key to lay the foundation for further simulations and analysis of the cutting process. Methods for surface roughness predictions have been proposed in, [1–3], utilizing time domain simulations which requires model based formulations of the tool tip frequency response. Stability aspects of the cutting process have also been addressed in the literature. The state where the cutting process experience uncontrolled vibrations is often referred to as chatter vibrations, a form of regenerative vibrations, which escalate in amplitude due to feed-back from the cutting process. To predict and optimise the cutting process, in which the avoidance of chatter is central, an accurate representation of the dynamic properties of the machine and cutting tool assembly is of the essence. Extensive research has been ongoing on the topic of chatter and regenerative vibrations in metal machining with pioneering work conducted in the 1960's by Tlustly [4] and Tobias [5]. Both [4] and [5] presented similar solutions to analytical expressions predicting the stability limit with respect to depth of cut of a turning operation. Their theoretical framework for turning operations were later developed further by Budak and Altintas [6, 7] to be applicable for milling as well. In their work, a dynamic milling model with directional dynamic milling force coefficients were introduced enabling an analytical solution that better considered the change

in direction of the cutting force in a milling operation. Their solution permitted a graphic presentation, known as stability lobe charts, of the stability limit with respect to spindle speed and depth of cut. The analytical solution to the stability problem in metal machining presented in [4–7] has the advantage that it can be established based on raw frequency response function (FRF) data directly and hence no system model identification is required. However, in order to establish such solution an assumption that the cutting forces have a linear dependency with respect to feed and depth of cut needs to be made. Unfortunately, this approximation is not always proper. Phenomena like cutting tool jumping in and out of cut during vibrations and relations between cutting force and chip thickness that are non-linear in their dependency, are examples that may alter the stability limit in a way that cannot be explained by the aforementioned analytical solution. A time domain stability chart, see references [8–17], is one way of permitting a non-linear solution of the machining stability yet such requires a system model and is more time consuming to establish.

First principle modelling approaches are often taken when dynamic analysis of mechanical components are conducted. However, the machine tool is a complex mechanical structure, with multi axial motion capabilities, see Figure 1. To enable such complex motion the machine tool is assembled with numerous mechanical joints. This makes it difficult to model with a finite element model (FEM) approach, since the dynamic properties at the interface of cutting tools are hard to foresee. This makes such approaches insufficiently accurate in prediction of the tool tip frequency response of the machine tool/cutting tool assembly. The most common way of obtaining the required FRFs at the tool tip is instead by resorting to experimental dynamic testing. The advantage is that the system flexibility and damping are embedded in the measured FRF and hereby accounted for. However, taking the experimental approach is not free from obstacles either. In the case of a process optimisation of a multi-operational machine tool, this approach requires physical testing of a multitude of machine-tool/cutting tool combinations. The downside to this is that the FRFs of all cutting tools of interest need to be established separately. This is due to the fact that the dynamic properties changes with the variation in geometric properties of the different cutting tools. Further, it also requires that the machine tool is taken out of operation during measurements which leads to loss of valuable production time.

A way of reducing measurement time is to utilise a technique called substructuring to synthesise the dynamic response at the tool tip, [18–26]. Here the advantage is that a mechanical system, in this case the machine tool with the mounted cutter, can be viewed as an assembly of subsystems. This approach allows the frequency response to be obtained from substructuring based on a mixture of measurements, modelling and analysis depending on what suits best to the substructure in question. The dynamic characteristics of the machine tool is therefore preferably obtained on an experimental basis while the less complex cutting tool can be modelled by first principle analytical beam models or finite elements.

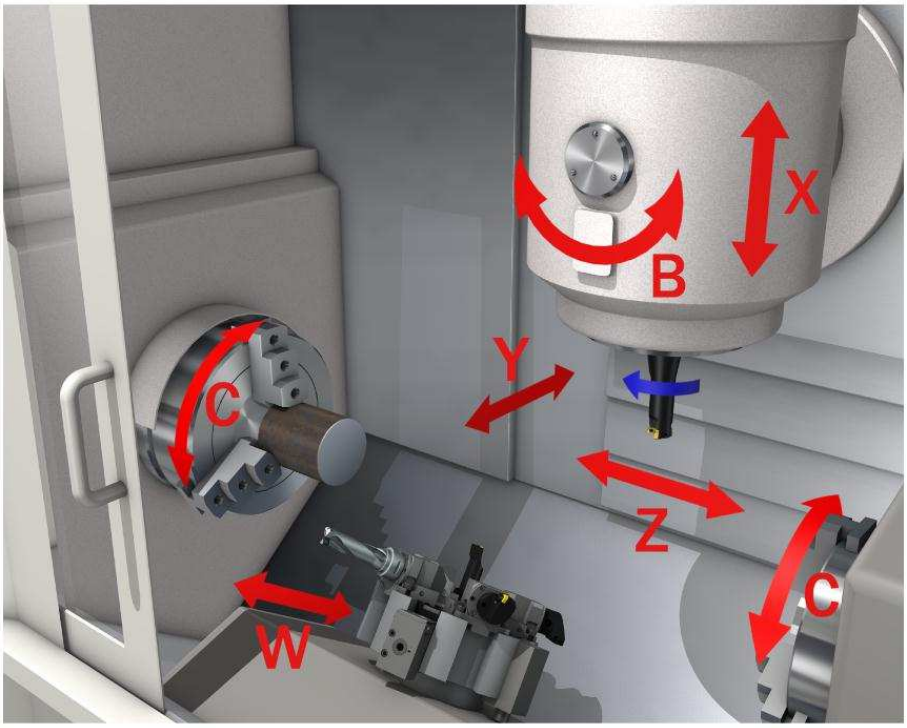

Figure 1: Machine tool with multi axial machining capability

Common for the substructuring approaches taken within this applied research field is that the coupling has been made on experimental data directly utilizing the classical frequency based substructuring (FBS) method by Jetmundsen *et al.* [27]. This method carries the advantage of modal completeness *i.e.* residual contributions from lower and/or higher frequency modes outside the measured interval is accounted for in the measurements which may be crucial for the coupled results, see Ewins [28]. However, it carries many well documented disadvantages. The method is sensitive to random noise, which is an ever present pollution in experimentally obtained FRFs, see Duarte [29]. The problem becomes imminent if the signal-to-noise ratio becomes small. Filtering techniques have been utilized, [22, 30], to smoothen the FRF which gives improvements of the coupled results. Yet other measurement artifacts can compromise the quality of the measured FRFs. Sensor collocation and orientation errors, McKelvey and Moheimani [31], as well as input-output signal truncation, Trethewey and Cafeo [32], may lead to severe errors in the coupled results. Relocated sensor mass between measurements, excitation device imperfections and accelerometer cable induced boundary conditions are other examples of non-noise errors affecting the measurements and in turn the coupled results.

1.1 Aim and scope

In this project, the use of a rational combination of experimental and analytical modelling is made to characterise the dynamic properties of the system. This approach may lead to a more time and cost efficient cutting tool development and cutting processes planing. The project aims at characterise the dynamic properties of the interface between the machine tool spindle and a cutting tool in a machine tool/cutting tool assembly where establishment of a model description that is fit for further analysis is a priority. The information about the spindle interface, in combination with FE-analysis of the cutting tool, will give the information needed for determining optimised design with a best set of cutting data to avoid regenerative vibrations. It will also give the possibility to predict tool tip response by time varying loads. The target is at maximising productivity, process stability and reliability and to reduce dynamic testing.

Characterisation of the spindle interface in the machine tool will here be done through inverse modelling of the dynamic behaviour. The characterisation of the dynamic properties at the interfaces between the tool and work piece will be made using system identification procedures. This information, together with *e.g.* finite element modelling of the tool, can be used to determine the cutting process parameters that give a chatter-free machining operation. In the sequel, this may be used for discussion of optimisation of productivity and cutting tool design.

2 Models in structural dynamics

Establishment of mathematical models representing structural components is often essential in product development. The models are key to evaluate and select product concepts at an early development stage before physical prototypes are produced and experimental testing begins. A preferred modelling format is often founded on first principles such as Newton's and Hook's laws where the model is based on laws of physics. This allows for deflection, stress and strain response analysis as the model is subjected to assigned load cases. The complexity of the model often grows with concept maturity, form rather simplistic analytical beam models, [33,34], that may be sufficient for early stage evaluation to complex FE models, Saabye and Petersson [35], as the project progresses.

2.1 Time domain modeling

Dynamic structural analysis of linear discrete physical models is often analysed using a second order ordinary differential equation (ODE) formulation, Craig and Kurdila [36], where the nodal displacement vector, $\{q\} \in \mathbb{R}^m$, m denoting the number of systems

degrees-of-freedom (DOF), is related to the load vector, $\{f\}$, by the symmetric mass, $\mathbf{M}$, viscous damping, $\mathbf{V}$, and stiffness , $\mathbf{K}$, matrices by

$$\mathbf{M}\{\ddot{q}(t)\} + \mathbf{V}\{\dot{q}(t)\} + \mathbf{K}\{q(t)\} = \{f(t)\} \tag{1}$$

As f is associated with the applied load at each DOF the load vector can preferably be rewritten using a matrix $\mathbf{P}_u$ to relate the applied stimuli vector, $\{u\} \in \mathbb{R}^p$ where p denotes the number of inputs, to a subset of DOFs

$$\{f(t)\} = \mathbf{P}_u\{u(t)\} \tag{2}$$

Similarly, it is also possible to selectively establish the displacement output, $\{y\} \in \mathbb{R}^r$ where r denotes the number of outputs, at a desired set of DOFs using

$$\{y(t)\} = \mathbf{P}_d\{q(t)\} \tag{3}$$

Provided that the mass matrix is non-singular, hence invertible, the second order formulation, Equation (1), lends itself to a reformulation into first order form known as state-space form

$$\begin{cases} \{\dot{x}(t)\} = \mathbf{A}\{x(t)\} + \mathbf{B}\{u(t)\} \\ \{y(t)\} = \mathbf{C}\{x(t)\} + \mathbf{D}\{u(t)\} \end{cases} \tag{4}$$

here $\{\dot{x}(t)\}$ is the n-dimensional state vector where $n = 2m$. The constant coefficient matrices quadruple $\{\mathbf{A}, \mathbf{B}, \mathbf{C}, \mathbf{D}\}$, holds the state matrix $\mathbf{A} \in \mathbb{R}^{n\times n}$, the input matrix $\mathbf{B} \in \mathbb{R}^{n\times p}$, the output matrix $\mathbf{C} \in \mathbb{R}^{r\times n}$ and the feed-through matrix $\mathbf{D} \in \mathbb{R}^{r\times p}$.

This structure is often preferred in control theory but is also very suitable in system identification of experimentally obtained model descriptions. The second order equation is cast in a first order form by introduction of the state vector

$$\{x(t)\} = \begin{Bmatrix} \{q(t)\} \\ \{\dot{q}(t)\} \end{Bmatrix} \tag{5}$$

and after some manipulation of Equation (1) with the extension of Equation (2) and introduction of the dummy equation $\{\dot{q}(t)\} = \{\dot{q}(t)\}$, see Gawronski [37], the state coefficient matrices in Equation (4) are made to relate to the second order form as

$$\mathbf{A} = \begin{bmatrix} \mathbf{0} & \mathbf{I} \\ -\mathbf{M}^{-1}\mathbf{K} & -\mathbf{M}^{-1}\mathbf{V} \end{bmatrix}, \quad \mathbf{B} = \begin{bmatrix} \mathbf{0} \\ \mathbf{M}^{-1}\mathbf{P}_u \end{bmatrix}, \quad \mathbf{C} = \begin{bmatrix} \mathbf{P}_d & \mathbf{0} \\ \mathbf{0} & \mathbf{P}_v \end{bmatrix} \tag{6}$$

where subscripts d and v relates to displacement and velocity respectively. The output equation, for selected displacements, y_d, and velocities, y_v, is

$$\{y(t)\} = \begin{Bmatrix} y_d(t) \\ y_v(t) \end{Bmatrix} = \begin{bmatrix} \mathbf{P}_d & \mathbf{0} \\ \mathbf{0} & \mathbf{P}_v \end{bmatrix} \{x(t)\} \tag{7}$$

As seen, the state vector in itself accommodates both displacement and velocity outputs hence the feed-through matrix $\mathbf{D}$ is only utilized when the state-space model output is acceleration. By noticing that accelerations are part of $\dot{x}(t)$, the relation for selected acceleration output, y_a, is thus obtained using the dynamic Equation (4) as

$$\{y_a(t)\} = \begin{bmatrix} 0 & \mathbf{P}_v \end{bmatrix} \mathbf{A} \{x(t)\} + \begin{bmatrix} 0 & \mathbf{P}_v \end{bmatrix} \mathbf{B} \{u(t)\} \tag{8}$$

which gives the direct throughput matrix for accelerations being $\mathbf{D} = [0 \quad \mathbf{P}_v]\,\mathbf{B}$.

2.2 Frequency domain modeling

In experimental structural dynamics the response is often studied and analysed in the frequency domain. The second order formulation in Equation (1) is taken to this domain by utilization of the Laplace transformation $f(t) = \mathcal{L}^{-1}\{F(s)\}$ with $s = j\omega$. This results in the following angular frequency, ω, dependant relation where j denotes the imaginary unit

$$\left[-\omega^2\mathbf{M} + j\omega\mathbf{V} + \mathbf{K}\right] \{\hat{q}(\omega)\} = \left\{\hat{f}(\omega)\right\} \tag{9}$$

or in a more compressed form as

$$\mathbf{Z}(\omega) \{\hat{q}(\omega)\} = \left\{\hat{f}(\omega)\right\} \tag{10}$$

The $\mathbf{Z}(\omega)$ matrix is known as the *dynamic stiffness matrix*. By Equation (10) it can be seen that the response vectors can be obtained from the force vectors by its inverse, $\mathbf{H}(\omega) = \mathbf{Z}(\omega)^{-1}$, as

$$\{\hat{q}(\omega)\} = \mathbf{H}(\omega) \left\{\hat{f}(\omega)\right\} \tag{11}$$

$\mathbf{H}(\omega)$, is also often denoted as the system's *receptance matrix* and its relation to the *stiffness* matrix will later be shown to be of importance in frequency based substructuring covered in section 3.2.1.

The first order form can be achieved in a similar manner as the defining frequency domain equation of stationary harmonic loading can be found from rewriting Equation

(4) using $\{u(t)\} = \{\hat{u}\}e^{j\omega t}$, $\{x(t)\} = \{\hat{x}\}e^{j\omega t}$, $\{y(t)\} = \{\hat{y}\}e^{j\omega t}$ and $\{\dot{x}(t)\} = j\omega\mathbf{I}\{\hat{x}\}e^{j\omega t}$ from which, after some manipulation, it follows that

$$\begin{cases} \{\hat{x}(\omega)\} = (j\omega\mathbf{I} - \mathbf{A})^{-1}\mathbf{B}\{\hat{u}(\omega)\} \\ \{\hat{y}(\omega)\} = \mathbf{C}\{\hat{x}(\omega)\} + \mathbf{D}\{\hat{u}(\omega)\} \end{cases} \tag{12}$$

From Equation (12) the generalised response and input are related as

$$\{\hat{y}(\omega)\} = \mathbf{C}\{\hat{x}(\omega)\} + \mathbf{D}\{\hat{u}(\omega)\} = \left[\mathbf{C}(j\omega\mathbf{I} - \mathbf{A})^{-1}\mathbf{B} + \mathbf{D}\right]\{\hat{u}(\omega)\} \tag{13}$$

hereby defining the frequency response transfer function $\mathbf{H}(\omega)$ to be

$$\mathbf{H}(\omega) \equiv \left[\mathbf{C}(j\omega\mathbf{I} - \mathbf{A})^{-1}\mathbf{B} + \mathbf{D}\right] \tag{14}$$

2.3 System identification

The structural dynamic model descriptions covered so far are often categorised as *internal*, or *white box*, models as they are based on first principles and physical properties to form system stiffness and inertia properties. Their ability to accurately model and predict behaviour of a physical component is hence determined by the accuracy in its physical properties and its description detail of the physical structure. As a product development project reaches its final stages and physical prototypes or component assemblies exists, the need for more detailed and accurate models increase. Even with very detailed product data it is sometimes hard, even with very comprehensive and high mesh density FE models at disposal, to appropriately model the behaviour of a very complex physical structure. The problem often lies in the dynamic properties of structural joints such as stiffness and especially the damping properties of these. In these cases it is sometimes better to resort to model descriptions based on experimental data from which the frequency response is established. For minor deviations between the experimental frequency response and that of an established *internal* model the solution to increase their correlation may be to resort to model updating, see Friswell and Mottershead, [38]. In such approach the physical parameters are altered, often in an optimisation fashion, until the model and measurement response better resembles each other. However, if the deviation is large this approach may not be easy. In that case, or if simply a relation between input and output at limited discrete locations are sought for, an *external*, or *black box*, model is more appropriate.

In the creation of an *external* model a system identification method is usually applied. The system identification aspect regards finding the best parameter estimate of a predefined model structure that accommodates measured input-output data, i.e. $[\{u\}, \{y\}]$. There exist many different methods for both time domain and frequency domain identification and extensive textbook literature can be found in [39, 40]. In

this thesis the system identification has exclusively been deployed by use of frequency domain data hence the subject will solely henceforth be covered in this domain.

The formulation of the frequency transfer function of the linear $[\mathbf{M}, \mathbf{V}, \mathbf{K}]$ system model in Equation (9) is often regarded as impractical in the establishment of an *external* model representation. The formulation is instead often recast into a description by modal superposition of the systems residues, A_{rpn}, and poles, λ_n, for details see Brandt [41], as

$$\mathbf{H}_{rp}(\omega) = \sum_{n=1}^{N} \left(\frac{A_{rpn}}{j\omega - \lambda_n} + \frac{\overline{A_{rpn}}}{j\omega - \overline{\lambda}_n} \right) \tag{15}$$

here N is the total number of system modes and an over-bar denotes the complex conjugate.

There are many different methods and commercial softwares available to estimate the residue and pole parameters and comprehensive coverage of experimental modal analysis can be found in [28, 42]. As the methods are many and the formulation in Equation (15) is not the model structure utilized in this thesis the coverage will only be brief. However, the general approach is to first determine the system poles that relate to eigenmodes. The number of modes within a measured frequency range is often unknown. To assist in determining a proper model order a useful tool is the mode indicator function, MIF. It basically exaggerates the global modes making their locations easier to find visually in graphs. Further, if the poles are located close to each other or if the experimental data are noisy the pole location selection can further be facilitated by utilization of a pole stabilization chart. Establishment of such have also been subject for much research and examples of experimental modal analysis algorithms are Polyreference Frequency Domain, (PFD) and Multi-reference Frequency domain, (MRFD) for multiple input multiple output, (MIMO), systems. For single input multiple output, (SIMO), systems the Least Squares Complex Exponential, (LSCE) is widely utilized. Figure 2 contains an example of a stabilization chart established using LSCE. In the making of Figure 2 the method was deployed for increasing state order of the numerical 7 DOF system provided in section 6.2. The MIF is plotted in the background and the probable pole locations appear as consecutive green dots along their designated frequency spectral lines. Hereby an assistance for the selection of pole locations is provided to the user. Once the poles have been determined the residues can be established by a least square pseudo inverse approach, for details see Maia [42].
In this thesis the model structure has been exclusively restricted to the state-space formulation on either mobility or receptance form. As such the direct throughput matrix $\mathbf{D}$ vanishes and the system identification aspect regards finding the most suitable matrix elements in $\mathbf{A}, \mathbf{B}$ and $\mathbf{C}$ to best capture the measured FRFs. To identify these matrix elements the common approach in **Papers A-E** has relied on the fre-

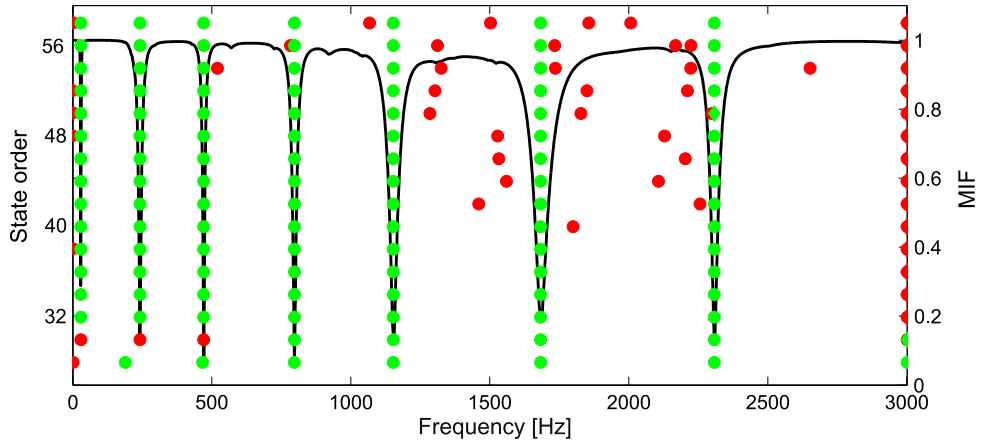

Figure 2: Example of stabilization diagram with embedded, MIF (black solid), possible physical mode (green dot), spurious mode (red dot)

quency domain system identification algorithm `n4sid`, by McKelvey *et al.* [43]. The experimental data imposes the issue of unknown model order to properly capture the system behaviour within the measured frequency interval. To address this matter an automated model order estimation algorithm as described by Yaghoubi and Abrahamsson [44] have been invoked in **Papers C-E**. The algorithm uses the identification algorithm, `n4sid`, in combination with a bootstrapping method for statistical evaluations to establish an appropriate state order. Further, all system identifications have been applied onto mobility FRF data and the reason is that the automated model order estimation algorithm has been found to perform at its best on mobility data since the FRF peak amplitudes are more equal over a wide range of frequencies compared to receptance or accelerance FRFs for the systems studied here.

3 Component synthesis theory

As a mixture of both *internal* and *external* models starts to accumulate within a product development project it is often convenient to model the complete structure by component synthesis of substructures. This methodology divides the structure into subcomponents which are modelled separately. Hereby, a more versatile modelling approach can be taken, where a mixture of experimentally and analytically obtained dynamic system representations can be combined to synthesise the assembled system. A variety of subsystem synthesis methods stands at disposal, each with different benefits and drawbacks. These methods have traditionally been divided into two main categories direct frequency response function based substructuring (FBS) and component mode synthesis (CMS).

3.1 Component mode synthesis, CMS

Component mode synthesis is often employed to couple models set up from physical first-principle laws such as FE models. The two most commonly used strategies by CMS, couple the subcomponents by either the fixed-interface or free-interface mode method. The utilisation of the fixed-interface mode method employing CMS were first conducted by Hurty [45] in the mid 1960s. The method he developed was later simplified by Craig and Bampton [46] which, instead of imposing that each interface DOF separately was required to be of rigid-body type or redundant interface type, regarded the interface DOFs together in a uniform setting. This made the method more accurate and more computationally efficient. The adjustments they made, made the method more suitable for FE implementation and it is today widely used within this field of simulations. The free-interface mode method was first introduced by Craig and Bampton in [47] which considered the component modes to be vibrating modes with free interface DOFs. The free-interface mode approach has also been taken by Rixen [48] providing a coupling method called Dual Craig-Bampton method which preserved the sparsity of the mass and stiffness matrices exhibited by the residual-flexibility matrix in lieu to the method put forward in [47]. The method presented in [48] proved to be more accurate than the Craig-Bampton method in terms of the estimating eigenfrequencies of the coupled system. A more thorough survey of the different CMS methodologies and theories can be found in the book by Craig and Kurdila [36] and de Klerk *et al.* [49] give a historical review on the subject.

3.2 Frequency based substructuring, FBS

This methodology is a coupled model synthesis based on frequency response models of each subcomponent. The frequency response models can be obtained either from synthesised modal models or from measured FRFs directly. The ability to use measured FRFs is one of the most distinguishing features of the FBS method compared to CMS. Modal analysis implications, such as model order and residual implications, see **Paper D**, can hereby be eliminated and contribution of high frequency modes can be accounted for since this information is embedded within the measured data. The fundamental idea of FRF based coupling originated from the impedance coupling method (IC) which describes the boundary DOFs at the joints between substructures by impedance matrices.

3.2.1 Impedance coupling method

With this method the information of kinematic constraints and equilibrium conditions between components are carried through the impedance matrix $\mathbf{Z}(\omega)$, and was first derived by Bishop and Johnson in [50]. They describe the force and displacement

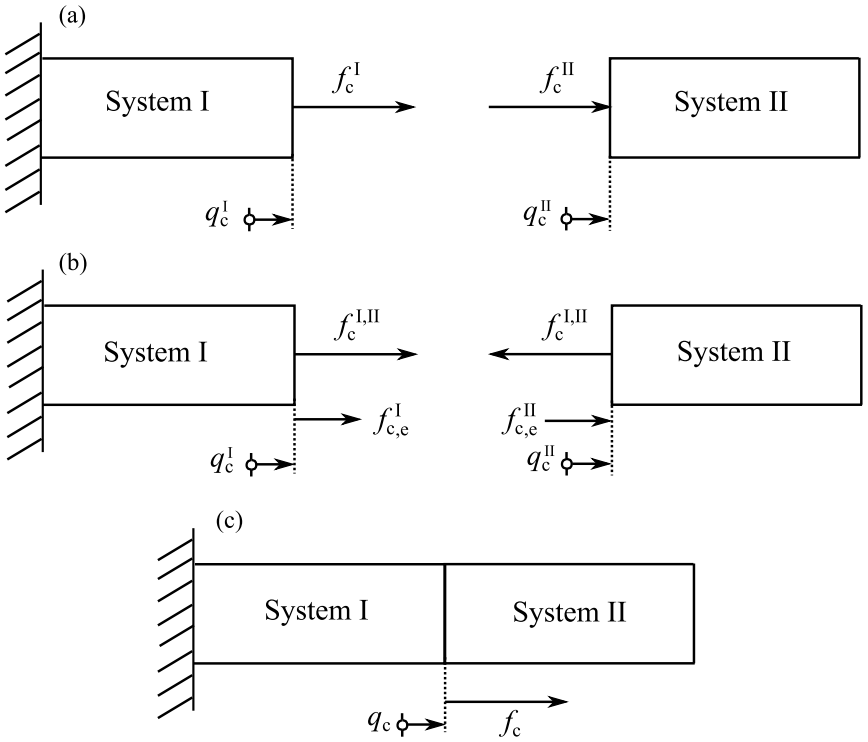

Figure 3: Illustration of coupling procedure. (a) Uncoupled subsystems I and II. (b) Kinematic and equilibrium constraints introduced. (c) Coupled system I+II

continuity through the coupling points between the assembled subsystems through the frequency dependant and complex-valued impedance matrix, Equation (10).

To utilise the impedance matrix in coupling of substructures it is needed to enforce compatibility and equilibrium conditions, see Figure 3. The generalised response co-ordinate of the assembled structure, q_c, has to be coincident with the coupling co-ordinates of the substructures to be assembled such that $q_\mathrm{c} \stackrel{def}{=} q_\mathrm{c}^\mathrm{I} = q_\mathrm{c}^\mathrm{II}$ and the total external load applied to the interface DOFs of the assembly has to fulfil the requirement that $f_\mathrm{c} \stackrel{def}{=} f_\mathrm{c}^\mathrm{I} + f_\mathrm{c}^\mathrm{II} = f_\mathrm{c}^\mathrm{I,II} + f_\mathrm{c,e}^\mathrm{I} - f_\mathrm{c}^\mathrm{I,II} + f_\mathrm{c,e}^\mathrm{II} = f_\mathrm{c,e}^\mathrm{I} + f_\mathrm{c,e}^\mathrm{II}$ where $f_\mathrm{c}^\mathrm{I,II}$ denotes the cross-sectional force between the two components and $f_\mathrm{c,e}^\mathrm{I}$ and $f_\mathrm{c,e}^\mathrm{II}$ are the externally applied forces to the interface DOFs of components I and II.

These conditions can be written in matrix form with use of the transformation matrix $\mathbf{T}$, for details see Ren and Beards [51], as

$$\{q_\mathrm{s}\} = \mathbf{T}\{q_\mathrm{c}\} \tag{16a}$$

$$\{f_c\} = \mathbf{T}^\mathrm{T}\{f_\mathrm{s}\} \tag{16b}$$

where subscript s refers to the co-ordinates on the substructure. With Equation (10) rewritten as a matrix equation of subsystems

$$\mathbf{Z}_{\mathrm{s}}(\omega)\left\{q_{\mathrm{s}}\right\} = \left\{f_{\mathrm{s}}\right\} \tag{17}$$

and with utilization of the compatibility and equilibrium conditions in Equation (16) a reformulation of Equation (17) can be established as

$$\left\{q_c\right\} = \left(\mathbf{T}^{\mathrm{T}}\mathbf{Z}_{\mathrm{s}}(\omega)\mathbf{T}\right)^{-1}\left\{f_c\right\} \tag{18}$$

From Equation (18) it can see that the receptance matrix of the assembled system $\mathbf{H}(\omega)$ corresponds to

$$\mathbf{H}(\omega) = \left(\mathbf{T}^{\mathrm{T}}\mathbf{Z}_{\mathrm{s}}(\omega)\mathbf{T}\right)^{-1} \tag{19}$$

This methodology fulfils all physical requirements needed through the compatibility and equilibrium conditions but it is numerically inefficient as the method requires two matrix inversions. First the subsystem receptance matrix $\mathbf{H}_{\mathrm{s}}(\omega)$ needs to be inverted to obtain the impedance matrix $\mathbf{Z}_{\mathrm{s}}(\omega)$ and then a full size matrix inversion of Equation (19) is required. The inversion of the matrices makes this method especially sensitive to measurement noise and matrix rank deficiencies which may cause significant errors in the coupled model.

3.2.2 Generalised FRF impedance coupling technique

An alternative method to the IC-method were developed by Jetmundsen *et al.* in [27] where the number of required matrix inversions was reduced to one. This methodology applied to coupling of two subcomponents, I and II, provides the following matrix equation

$$\mathbf{H} = \begin{bmatrix} \mathbf{H}^{\mathrm{I}}_{\mathrm{cc}} & \mathbf{H}^{\mathrm{I}}_{\mathrm{co}} & 0 \\ \mathbf{H}^{\mathrm{I}}_{\mathrm{oc}} & \mathbf{H}^{\mathrm{I}}_{\mathrm{oc}} & 0 \\ 0 & 0 & \mathbf{H}^{\mathrm{II}}_{\mathrm{oo}} \end{bmatrix} - \begin{bmatrix} \mathbf{H}^{\mathrm{I}}_{\mathrm{cc}} \\ \mathbf{H}^{\mathrm{I}}_{\mathrm{oc}} \\ \mathbf{-H}^{\mathrm{II}}_{\mathrm{oc}} \end{bmatrix} \left(\mathbf{H}^{\mathrm{I}}_{\mathrm{cc}} + \mathbf{H}^{\mathrm{II}}_{\mathrm{cc}}\right)^{-1} \begin{bmatrix} \mathbf{H}^{\mathrm{I}}_{\mathrm{cc}} \\ \mathbf{H}^{\mathrm{I}}_{\mathrm{oc}} \\ \mathbf{-H}^{\mathrm{II}}_{\mathrm{oc}} \end{bmatrix}^{\mathrm{T}} \tag{20}$$

where $\mathbf{H}$ is the synthesised assembled receptance matrix and subscript (c) and (o) denotes interface and other DOFs respectively. It should be noted that the notation of $\mathbf{H}(\omega)$ and $\mathbf{Z}(\omega)$ have been changed to $\mathbf{H}$ and $\mathbf{Z}$ for brevity yet it is still implied that $\mathbf{H}$ and $\mathbf{Z}$ are frequency dependent. A more general derivation of Equation (20) was conducted by Ren and Beards in [51] to further utilise the concept of graph theory and mapping matrices, presented in [27] and [52] for the boolean operation of an arbitrary

number of substructures. The generalised FRF impedance coupling technique and the coupling formulation in Equation (20) have been utilized in **Papers B** and **E** for evaluation purposes against the coupled results of state-space component synthesis.

3.3 State-space based coupling

The substructure synthesis method used to couple subcomponents in **Papers A, B** and **E** with improvements suggested in **Papers C** and **D**, has been the state-space based coupling technique proposed by Sjövall [53]. The state-space based coupling methodology is closely related to FBS in that identical kinematic and equilibrium constraints are enforced on the coupling. The state-space method approach to couple substructures was first taken by Su and Juang in [54] arguing several advantages compared to FRF-based coupling methods. Some of the more prominent advantages enlightened by [54] were the avoidance of ill-conditioned matrix inversions of the FRF matrices and simplicity in identification on subsystem level with the estimation of several lower order models. This is made rather than estimating a higher order model that is required for the coupled system level. The state-space based coupling method proposed by [53] distinguishes itself from the method given by [54] in that it applies proper similarity transformations of the subsystem state-space models in lieu to [54] that instead proposed an introduction of two additional auxiliary state variables to each interface DOF. The method is described in fuller detail in **Paper B**.

4 Machining dynamics by component synthesis

Stability analysis for increased productivity and process reliability is used within the metal machining industry. However, the use is to some extent limited by a number of factors. The methodology to employ stability lobe analysis requires experienced users to conduct the measurements of system transfer functions and to carry out the stability analysis. The use of the methodology is also affected by the requirements on the measurement procedure. To obtain the correct dynamic flexibility at the tool tip for a specific cutting tool it is required that the cutting tool is mounted in the machine tool of interest at test time. The use of a test rig or a FE representation of the machine tool have been proven insufficient in order to obtain the correct damping and stiffness parameters of a machine tool. This is mainly due to the mechanical joint complexity of the machine tool structure. Furthermore the test procedure requires that the machine tool has to be taken out of operation during measurement. This results in loss of valuable production time. The productivity loss during measurements of a machine tool mounted cutting tools can be expensive for larger production plants. Large production facilities can be equipped with more than 30 machine tools where each machine tool may carry a substantial amount of cutting tools due to the modularity of today's tooling concepts, see Figure 4.

In an effort to reduce measurement time a number of researchers, see [18–26], have utilised component synthesis to obtain the dynamic flexibility of a machine tool mounted cutting tool. The approach to the problem is to regard the cutting tool and the machine tool as two separate subsystems and then deploy component synthesis to construct the FRFs of transversal motion at the tool tip which are required for the stability lobe prediction. Dividing the machine tool/cutting tool assembly into subcomponents allows system identification to be conducted on subsystem level. This means that the measurements of the machine tool dynamics only have to be conducted once. The system description of the cutting tool, which is a less complex mechanical component, is normally made using analytical models of the tool in studies reported.

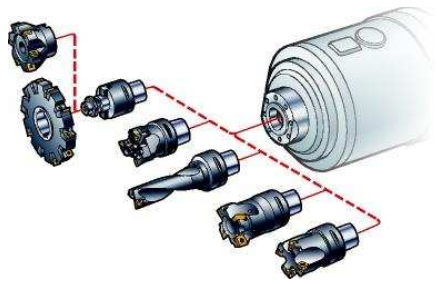

Figure 4: Machine tool modularity. This figure shows seven cutting tools but a magazine of a machine tool can hold up to over 100 cutting tools.

The substructuring approach to predict the tool tip dynamics was first taken by Schmitz and Donaldson [18]. The coupling was made on the measured machine tool subcomponent FRFs to the analytically obtained FRFs of the free-free cylindrical cutting tool substructure directly utilizing the generalised FRF impedance coupling technique. In their work, the rotational degree of freedoms (RDOFs) were neglected in the experimental characterisation of the coupling between the machine tool/tool holder subcomponents. An interface flexibility between the two subassemblies were instead introduced to compensate for the assumed joint flexibility between the tool holder and cutting tool. The introduction of the interface flexibility required an additional measurement of a representative machine tool/tool holder mounted cutting tool to calibrate the interface flexibility properties. Their work was extended to include the RDOFs reported in Schmitz *et al.* [19]. However, these theoretical extensions were not validated due to the absence of reliable measurement techniques of the RDOF FRFs.

The problem to obtain the RDOFs at the connection point on the machine tool substructure side was addressed in Park *et al.* [20]. Park made a different substructure partition than made in [18, 19], by mounting a small part of the cutting tool inside the tool holder. A measurement procedure was proposed that allowed the RDOFs to be obtained by measurements conducted on two blank calibration cylinders. The proposed procedure was to conduct impact testing on one short blank cylinder and one longer blank cylinder and then calculate the RDOFs at the free end of the short blank based on these measurements using a decoupling procedure. The cutting tool FRFs at the connection point were then constructed using an FE model of a cylindrical beam coupled to connection point on the machine tool/tool holder/blank substructure. This approach was later adopted by Namazi *et al.* [55] to retrieve the RDOFs closer to the machine tool spindle interface. This was achieved by partitioning the machine tool and a small part of the tool holder as one substructure and the tip of the tool holder and cutting tool as the other by applying the same experimental and decoupling methods as proposed in [20]. The method proposed by Park has been benchmarked in **Paper E** and the reader is referenced to that paper for further insight.

An alternative approach to retrieve the RDOFs at the connection point between machine tool side of the substructures was taken by Schmitz and Duncan [22]. The methodology they proposed included a triple-component coupling strategy where the machine tool and the base geometry of a tool holder were considered as one combined substructure. The tip of the tool holder with the inserted part of the cutting tool constituted another substructure and the part of the cutting tool outside of the tool holder was the third substructure. To obtain the RDOFs about the connection point between the machine tool and tool holder base and the tip of the tool holder they proposed a two step method. It consists of a first step in which measurements on the translational DOFs at the free end of a machine tool mounted representative

tool holder were conducted. Then the RDOFs were calculated based on a receptance decoupling method, from which the part of the general tool holder from the base to the tip was subtracted. From these the machine tool/tool holder base receptances could be obtained. In this work a synthesis of the RDOFs based on FRF data is also proposed. This approach has also been subject of investigation in the benchmark problem presented in **Paper E**

A filtering method was applied in [22] to the measurements of the machine tool/tool holder with the aim to minimise the noise influence. The implication of noise contaminated measurements on coupling of machine tool/cutting tools was further investigated by Schmitz and Duncan in [24]. They concluded that the noise contamination may strongly influence the results due to the matrix inversion made during the coupling of the FRFs. In Park and Chae [25] the approach on flexible joint description taken by Schmitz and Donaldson was combined with the method in [20] to account for the transfer function associated to the RDOFs of joints located adjacent to the tool tip. In [25] it was showed that this approach further could enhance the accuracy of the model of the coupled system.

4.1 Cutting tool model

In early substructuring attempts the cutting tool representations were made using cylindrical beam models with a reduced diameter to compensate for the fluted geometry on solid carbide cutting tools. The influence of fluted geometry was addressed by Kivanc and Budak [56] where a derivation of moment of inertia considering 2, 3 and 4 straight fluted solid carbide geometries was presented. The advantage of using Timoshenko beam models rather than Euler-Bernoulli beam models to represent the cutting tool substructure was stressed in Erturk *et. al.* [23]. The advantage with the Timoshenko representation over the Euler-Bernoulli formulation is that the rotary inertia and the shear deformation is considered. Especially the shear deformation is important to consider to increase accuracy in the calculated eigenvalues for cutting tools with small length-to-diameter ratio, for details see Timoshenko *et al.* [33]. The analytical approach utilizing Timoshenko formulation of straight fluted cutting tools was further developed by Mancisidor *et al.* [57], proposing a novel method utilizing a combination of clamped free and rigid body modes to establish a free-free representation of the cutting tool. They showed that the number of modes required could be drastically reduced yet maintaining a high level of accuracy in the coupled results. Solid carbide cutting tool flutes are almost always helical to their design as the helical shape facilitates ship evacuation and reduces sound levels in the cutting process. The helical shape was taken into consideration by Özşahin and Altintas who utilized the moment of inertia description by Kivanc and Budak and divided the tool into discrete segments with fixed cross-section along the axial direction of the cutter. The

helical shape was approximated by sequential rotation of each segment and which also permitted for variations in flute cross section at different locations of the cutter.

The tool tip modelling approach taken in the appended **Papers B** through **E** distinguishes itself from the approaches described which sits best for solid carbide tools. The solid carbide tool segment is indeed important but is small compared to sales of indexable cutting tool. Indexable cutting tools often consists of a steel body on to which small inserts are mounted. These inserts are active in the cutting process and can consist of a variety of different materials such as coated solid carbide, ceramics, cubic boron nitride and in some cases even polycrystalline diamond. As the insert is worn down by machining, it is simply replaced by a new providing a more economical tooling solution. An indexable cutting tool body differs, in some cases a lot, from the rather continuous shape of a solid carbide cutter and to account for these variations the modelling approach has been based on appropriate FE models based on the CAD models to represent its complex geometry. A CAD and FE model approach is slower than a strictly analytical approach with representative beam models but it enables a more versatile analysis of tool geometric alterations in studies of the substructure response.

4.2 Substructure partition

Many of the articles cited within this application field have regarded flexible joints as a part of the modelling description. The necessity of such local flexibility is governed by the cutting tool design and the localisation of the interface between the cutting tool and machine tool. A short example will be provided to illustrate the splitting aspect and how joint identification at the spindle and tool holder interfaces can be circumvented. Consider the defined system assembly in Figure 5.
The presented structure is an extreme simplification of a machine tool, tool holder and cutting tool assembly, yet it is still valid to motivate the partitioning strategy

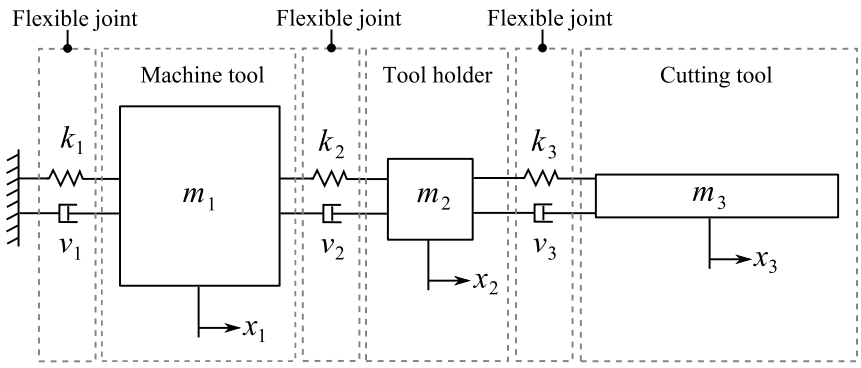

Figure 5: Assembly model

Table 1: Physical parameter values of damping and stiffness elements

i	1	2	3
m_i [kg]	1	1	1
v_i [Ns/m]	110	20	70
k_i [kN/m]	3095	9870	9870

taken in this thesis. As seen, the simplified structure consists of three discrete inertia elements, representing the machine tool, the tool holder and the cutting tool. Each of them are sequentially connected with linear spring and damper elements and with a set of spring and damper element connected between the machine tool and ground. The intermediate stiffness and damper elements between the inertia represent flexible joints. The flexible joint between the machine tool spindle interface and tool holder has been subject of investigation in Namazi *et al.* [55] and is represented by stiffness and damping k_2 and v_2 and the joint flexibility between the tool holder and cutting tool is represented by k_3 and v_3 in investigations presented in [18, 19, 21, 22].

To enable a construction of the examples illustrating the different partitioning strategies a reference system (True) is established based on the assigned joint elements values in Table 1 and the formation of the mass, stiffness and damping matrices as

$$\mathbf{M}^{\text{True}} = \begin{bmatrix} m_1 & 0 & 0 \\ 0 & m_2 & 0 \\ 0 & 0 & m_3 \end{bmatrix}$$

$$\mathbf{V}^{\text{True}} = \begin{bmatrix} v_1 + v_2 & -v_2 & 0 \\ -v_2 & v_2 + v_3 & -v_3 \\ 0 & -v_3 & v_3 \end{bmatrix}, \quad \mathbf{K}^{\text{True}} = \begin{bmatrix} k_1 + k_2 & -k_2 & 0 \\ -k_2 & k_2 + k_3 & -k_3 \\ 0 & -k_3 & k_3 \end{bmatrix} \tag{21}$$

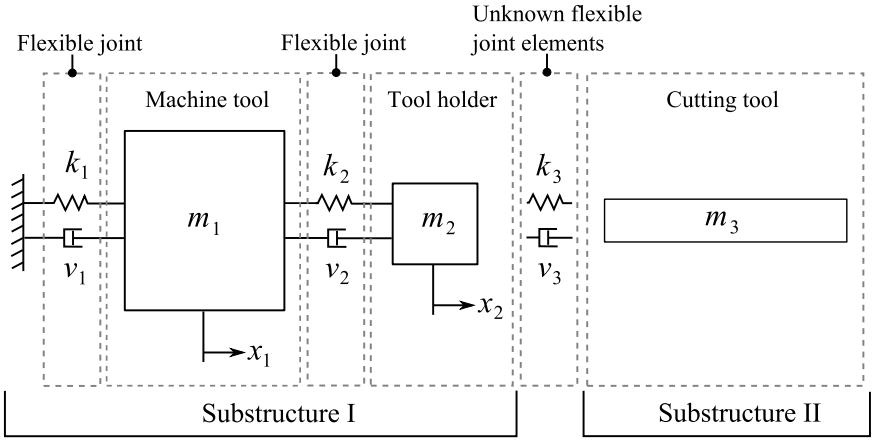

Figure 6: Numerical substructure partition: Machine tool/tool holder as substructure I and cutting tool as substructure II

4.2.1 Machine tool/tool holder partition

A convenient substructure partition is to consider the machine tool and tool holder as one substructure and the cutting tool as a second substructure, see Figure 6. A partitioning scheme such as this is attractive since it requires no splitting of existing physical components. However, it has a downside in that the joint parameters between the tool holder and the cutting tools cannot be obtained in a single measurement session and need to be obtained through additional testing and joint parameter calibrations.

The necessity of additional testing will be illustrated in the following example. The dynamic characteristics of the machine tool structure is, as previously argued, preferably obtained by testing. In such testing, the machine tool mounted tool holder is normally subjected to a short force impulse at DOF 2 (x_2). In practice this is often made by hammer excitation. For this example the impulse is constructed using an ideal pulse filtered using a lowpass 2:nd order Butterworth filter with a cut-off frequency of 3000 Hz. The filtered impulse and the system response are sampled at a rate of, $f_s = 1$ MHz and the response is obtained using a digital filter representation of the system and ramp invariant transformation as proposed by Ahlin *et al.* [58], see Figure 7.

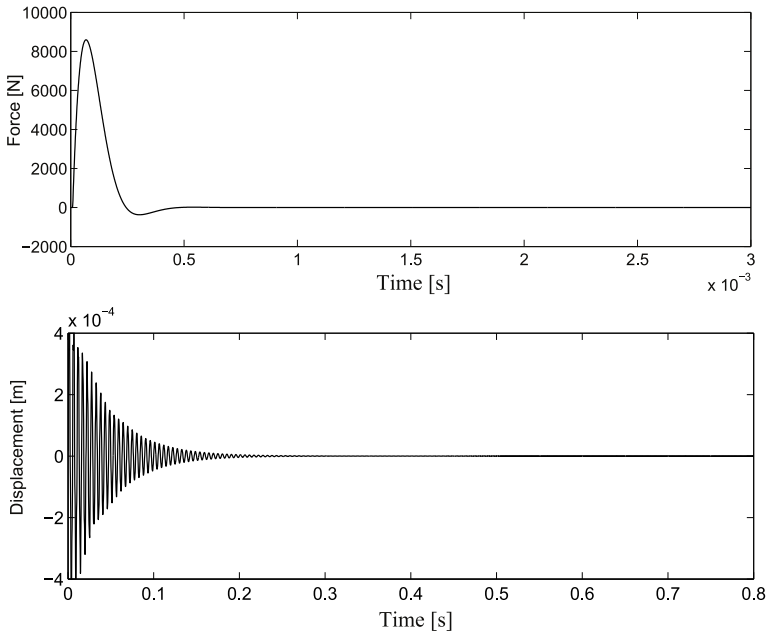

Figure 7: Upper: impulse input at DOF 2. Lower: computed response at DOF 2

To mimic the practical situation, the transfer function of the system is estimated from these calculated input and output signals. This synthetic experiment gives the possibility of comparing with the true system transfer function. Based on the calculated force and response the FRF is established by `Matlab`'s algorithm `tfestimate` which is based on Welch's averaged, modified periodogram method [59], using a response capture time of 0.8 seconds. The established FRF, H_e^{I}, is compared to the true FRF, H_r^{I}. The true FRF of the free-free cutting tool mass, H_r^{II} is also given in Figure 8. The two true transfer function of the two systems (substructure I and substructure II) have been established using Equation 22 and the parameter values given by Table 1.

$$\mathbf{H}\left(\omega\right) = \left(-\omega^2\mathbf{M} + j\omega\mathbf{V} + \mathbf{K}\right)^{-1} \tag{22}$$

where the mass, stiffness and damping matrices are of substructure I are

$$\mathbf{M}^{\mathrm{I}} = \begin{bmatrix} m_1 & 0 \\ 0 & m_2 \end{bmatrix}, \quad \mathbf{V}^{\mathrm{I}} = \begin{bmatrix} v_1 + v_2 & -v_2 \\ -v_2 & v_2 \end{bmatrix}, \quad \mathbf{K}^{\mathrm{I}} = \begin{bmatrix} k_1 + k_2 & -k_2 \\ -k_2 & k_2 \end{bmatrix} \tag{23}$$

and substructure II consists of the single free-free mass inertia element, m_3.

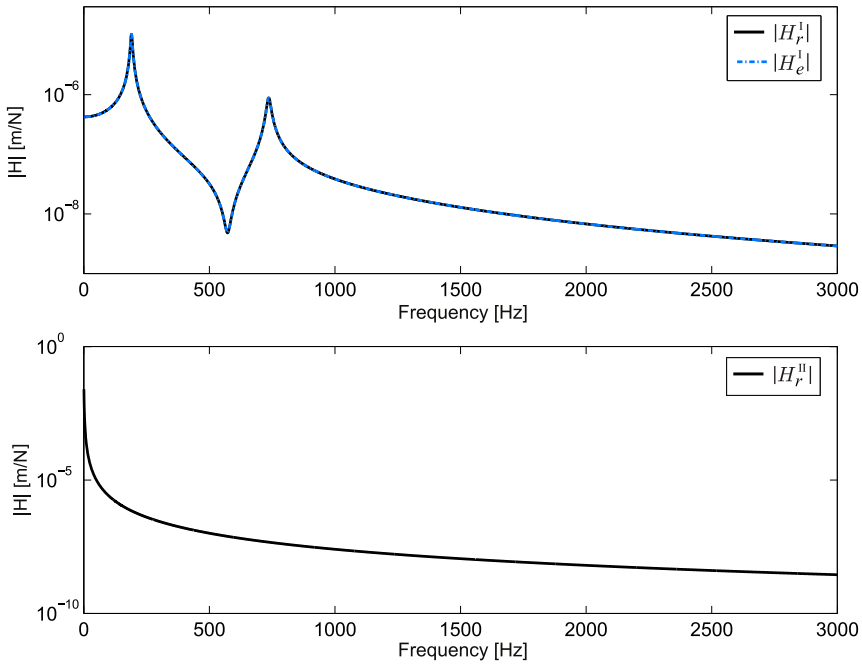

Figure 8: FRFs at coupling DOFs: Upper figure contains the true theoretical FRF, H_r^I, and experimentally obtained FRF, H_e^I. Lower figure contains the theoretical FRF of the free-free substructure II

As seen in Figure 8 in the comparison the correlation is good between the true and the estimated FRFs of substructure I. The purpose of this comparison is to underline that the structural flexibility, including the structural flexible connection to ground and between spindle and tool holder, is embedded in the measured FRF.

As the joint information between the holder and cutting tool is missing the shortcoming of the experimental procedure becomes obvious by coupling of H_e^I and H_r^{II} using Equation 20 and studding coupled results in comparison to the true assembled system by applying $\mathbf{M}^{\mathrm{True}}$, $\mathbf{V}^{\mathrm{True}}$ and $\mathbf{K}^{\mathrm{True}}$ to Equation 22, see Figure 9. Connecting the two substructures without considering the flexibility of the joint results in an assembled structure that is stiffer than the true systems. As such the system resonances are located at higher frequencies which in turn influences the accuracy of further cutting process simulations and analysis.

An experimental set-up such as this hence requires that intermediate flexible joint elements are introduced between the tool holder and the cutting tool and that these elements are calibrated using additional testing of a fully assembled structure, see [18, 19, 21, 22]. Once this is completed, substructuring of other cutting tools onto the machine tool/tool holder substructure can come in question.

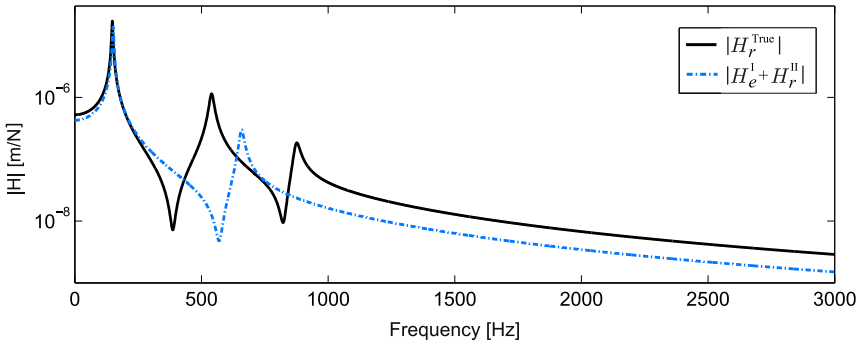

Figure 9: Comparison of synthesis of, H_e^I and H_r^{II}, and true assembled structure H_r^{True}

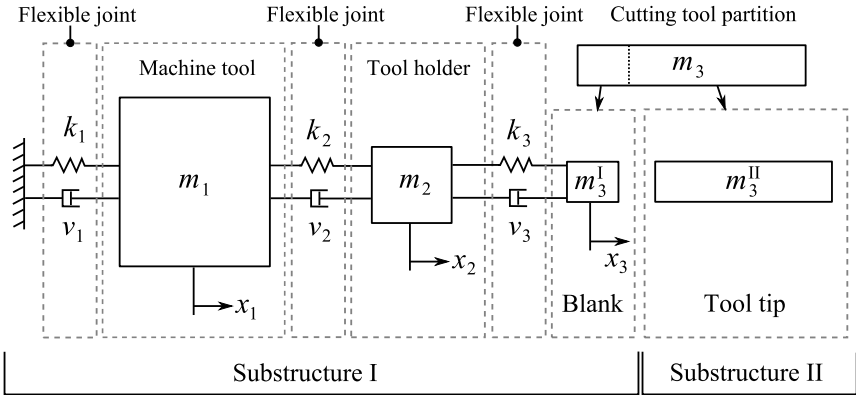

Figure 10: Numerical substructure partition with integrated cutting tool partition

4.2.2 Integrated cutting tool partition

The problematic aspect regarding the missing joint description in the previous section can be circumvented by adding a small portion of the cutting tool to the machine tool/tool holder substructure partition, see Figure 10. This approach was first taken in [20] and has been the substructure partition strategy taken in **Papers A-E**.
The benefit by this approach can be exemplified by adding a small part of the cutting tool mass element, $m_3^{\text{I}} = 0.1$ [kg], (here named blank) to the machine tool/tool holder configuration. This corresponds to partitioning the cutting tool and mouthing the blank section in the tool holder. Next the example is continued by applying the same input force as presented in Figure 7, to DOF 3 of substructure I, calculate the response and establish the FRFs in a similar fashion as presented in the previous section. By this partition the stiffness and damping matrices of substructure I are $\mathbf{V}^{\text{I}} = \mathbf{V}^{\text{True}}$ and $\mathbf{K}^{\text{I}} = \mathbf{K}^{\text{True}}$ and the mass matrix $\mathbf{M}^{\text{I}}$, is

$$\mathbf{M}^{\mathrm{I}} = \begin{bmatrix} m_1 & 0 & 0 \\ 0 & m_2 & 0 \\ 0 & 0 & m_3^{\mathrm{I}} \end{bmatrix} \tag{24}$$

and substructure II consists of the single free-free mass inertia element, $m_3^{\mathrm{II}} = 0.9$ [kg], of the partitioned cutting tool mass.

The results of this procedure is provided in Figure 11. As seen, the experimentally obtained FRF now consists of 3 modes as the joint flexibility between the tool holder and the cutting tool is considered in the experimental configuration (substructure I). By assembling substructure I and II it is now found that the match is good between the synthesised FRF and the calculated true system, see Figure 12.

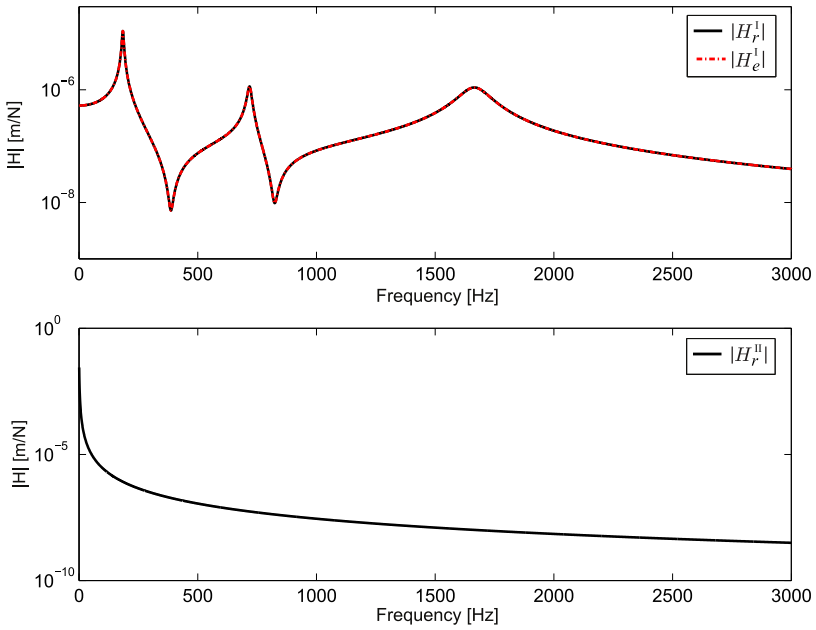

Figure 11: FRFs at coupling DOFs: Upper figure contains the true theoretical FRF, H_r^I, and experimentally obtained FRF, H_e^I with integrated tool partition. Lower figure contains the FRF of the free-free partition of the cutting tool (substructure II)

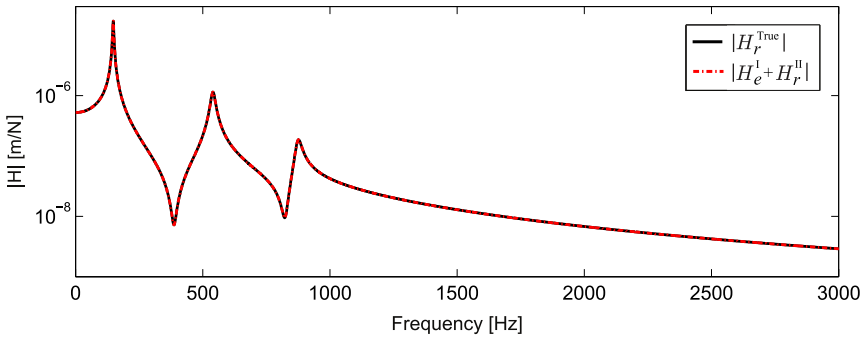

Figure 12: Comparison between substructured results of, H_e^I and H_r^{II}, and true fully assembled structure H_r^{True}

As stated before the two examples presented here are extremely simplistic. In substructuring of a physical machine tool and cutting tool configuration both translational and rotational DOFs need to be considered to appropriately capture the dynamic properties at the coupling interface. The integrated cutting tool partition eliminates the need for joint identification between the machine tool-tool holder-cutting tool but it does not eliminate the need for joint identification for all machine tool cutting tool combinations. In configurations with joints near the tip of the tool, see Figure 13, a tool tip adjacent joint identification still have have to be considered as suggested by Park and Chae [25]. No flexible joint descriptions has been considered in this thesis as no tooling solution of the sort where the joints of the substructures could not be integrated in the experimental data have been considered. The focus has been on robustness of the substructuring approach and on previously overlooked erroneous phenomenons and inconsistencies with physical principles.

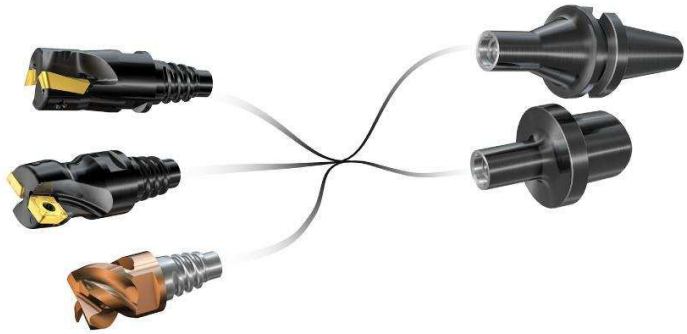

Figure 13: Example of cutting tool solutions with joint adjacent to tool tip

5 Motivation to the state-space approach

Setting out from a numerical dynamic representation of sub-structures will result in the same FRFs of the assembled structure using either one of the three approaches, CMS, FBS or state-space substructuring, see **Papers B** and **D**. The basic motivation to the used state-space approach is found in experimental obstacles that need to be tackled and the ability to immediately utilize the coupled system model for analysis. This can be done in both time domain analysis of the cutting process and for analytical stability lobe predictions. In experimental dynamic substructuring several obstacles arise due to the inability to properly measure the dynamic characteristics of the subsystems. Depending on which coupling method that is used these obstacles become more or less troublesome. Some of these obstacles have been mentioned above but will be covered more in detail here.

5.1 Noise free data

As stated one of the most prominent features using FBS is that it can be applied directly onto measured data. This has been the most common approach in the field of machining dynamics by component synthesis. As much as this is a strength it is also a weakness in the sense it puts rather high demands on the quality of the measured data. To assure a robust and reliable coupled result the FRF data representations should be free from noise, [28,29]. As mentioned in section 4, Schmitz and Duncan [22], utilized data filtering to smooth the measured FRFs. Data smoothing is a well documented technique to improve the accuracy and robustness of FBS. However, in the work by Imregun *et al.* [60], it was shown that it is beneficial to have one *consistent*, reciprocal modal model representation of the measured FRFs more so than fitting models to the individual FRFs. A state-space formulation provides one such platform where a MIMO-FRF matrix could be identified and hereby also alleviating the noise effect.

5.2 Rotational degrees of freedom, RDOF

An appropriate description of the dynamic response of a structure requires both translational and rotational DOF receptance formulation, Ewins and Gleeson [61]. However, measurements of the RDOFs are rather cumbersome. Examples of cases where RDOFs have been omitted can be found in literature, [20, 62]. These studies showed that significant errors in amplitude and resonance frequency prediction of the coupled system may occur if the RDOFs were excluded. The problematic aspect lies in the practical problem to measure rotational response directly since there are no rotational sensors on the market. A practical problem to obtain the full receptance is also the problem of applying a torque excitation to the structure at a single point of interest. An appropriate coupling point matrix contains FRFs of drive point and cross-coupling FRFs and can be subdivided in to four groups based on their input

and output characteristics. This is illustrated by the partition of the transfer function matrix $\mathbf{H}$ as

$$\mathbf{H} = \begin{bmatrix} \mathbf{H}_{\mathrm{TF}} & \mathbf{H}_{\mathrm{TM}} \\ \mathbf{H}_{\mathrm{RF}} & \mathbf{H}_{\mathrm{RM}} \end{bmatrix} \tag{25}$$

Here subscripts T and F denotes response and excitation force respectively associated to linear motion while R and M correspond to rotational response and moment excitation around a point. As seen in Equation (25), either a rotational excitation and/or response make up three quarters of the FRF matrix hence omitting the RDOFs results in significant information loss. Studies investigating the effect of excluding RDOFs in substructure coupling analysis have been reported in [62–64] and in experimental dynamic substructuring of machine tool in particular in [20]. From these studies it can be concluded that the RDOFs need to be included. This topic has been of interest to the experimental dynamic substructuring community for a long time and to some degree still remains to be.

A number of different approaches could be found in the literature that aim to measure the rotational responses as in the work by Bokelberg *et al.* [65,66]. A multi-directional transducer was developed, permitting response measurements in 6-DOFs by utilization of a laser vibrometer configuration with three laser beams. A similar strategy is the finite difference, (FD), approach which estimates the rotational response using differentiation between closely spaced accelerometers, [28,63]. As these approach only serves to fill the first block column elements in Equation (25), complementary strategies need to be applied to synthesise the moment input elements. These right column elements, $\mathbf{H}_{\mathrm{RM}}$, can be synthesized by identification of a *consistent* model representation and model expansion, Avitabile and O'Callahan [67]. As the state-space model permits for model expansion the FD approach in combination with model expansion have been the most frequently used approach in **Papers A-E**. However, other methods to synthesise the moment input elements using measured data directly can be found in the literature. Such approaches are often associated with a structural modification, [20, 28, 68] where an additional component is attached to the experimental substructure during testing. One of the more popular approaches is to attach a T-block to the experimental structure hereby allowing for both translational excitation and response to be measured at the ends of the T-block and the rotational response and moment input can be synthesized by decoupling of the T-block. The structural modification method in [20] has been benchmarked in **Paper E** indicating high sensitivity to model properties of the decoupled modification structure and measurement accuracy.

6 Experimental uncertainties

The substructuring approaches presented have different strengths and weaknesses and they all share a common obstacle in measurement errors and uncertainties. The noise issue have already been covered but errors such as sensor cross-axis sensitivity, calibration errors and relocated sensor mass between measurements also need to be considered. In testing with shakers with stinger, stinger imperfections induce uncertain boundary conditions that contribute to uncertainties in the coupled results. Accelerometer mass and vibrating cables also participate to inaccuracies. These errors and inaccuracies are preferably addressed during the experimental work however, some of them may be hard to acknowledge and avoid in an industrial experimental environment. One of the more important topics of this thesis is the establishment of physical consistent substructure models that partly adjust for experimental deficiencies by avoiding model fitting to experimental data which are in conflict with physical principles.

6.1 Test results inconsistent with principles of physics

Raw test data are usually processed by signal processing procedures. This may lead to frequency response data estimates that are inconsistent with established fundamental principles of physics. This subject, and its effects, have been sparsely covered in the field of experimental substructuring. Among the first to acknowledge the phenomenon were Carne and Dohrmann [69] who found that small measurement anomalies could have drastic effect, as spurious peaks frequently appeared in the frequency spectra of the coupled system. The artifacts in the estimated FRF are often hard/impossible to find by simply studying the absolute value of the measured FRF but from close examination of the real and imaginary parts of driving point FRFs these anomalies could often be located. In [69] comparisons are made between experimental and theoretical accelerance MIMO FRF. Let the accelerance be represented by its real and imaginary parts as

$$\mathbf{H}_{ij}^{a}(\omega) = \Re\left(\mathbf{H}_{ij}^{a}(\omega)\right) + j\Im\left(\mathbf{H}_{ij}^{a}(\omega)\right) \tag{26}$$

Based on real normal modes φ and natural frequencies ω_n the real and imaginary parts are (see [36])

$$\Re\left(\mathbf{H}_{ij}^{a}\left(\omega\right)\right) = -\omega^2 \sum_{n=1}^{N} \frac{\phi_n^i \phi_n^j \left(1 - \left(\frac{\omega}{\omega_n}\right)^2\right)}{K_n \left(\left(1 - \left(\frac{\omega}{\omega_n}\right)\right)^2 + \left(2\zeta_n \frac{\omega}{\omega_n}\right)^2\right)} \tag{27}$$

and

$$\Im\left(\mathbf{H}_{ij}^{a}\left(\omega\right)\right) = \omega^2 \sum_{n=1}^{N} \frac{\phi_n^i \phi_n^j \left(2\zeta_n \left(\frac{\omega}{\omega_n}\right)\right)}{K_n \left(\left(1 - \left(\frac{\omega}{\omega_n}\right)\right)^2 + \left(2\zeta_n \frac{\omega}{\omega_n}\right)^2\right)} \tag{28}$$

with K_n and ζ_n being the positive modal stiffness and damping respectively. By examining the imaginary part it can be seen that the drive-point FRFs, *i.e.* when $i = j$, is positive if $[\omega, K_n, \zeta_n] > 0$. Further this implies that the phase of $\mathbf{H}_{ij}^{a}$ is bounded to stay between $[0°, 180°]$. As the frequency response can be represented in mobility and receptance output as well the phase constraints for driving point FRF changes to $[-90°, 90°]$ and $[-180°, 0°]$ respectively and from being positive imaginary in the accelerance case, to positive real in mobility and negative imaginary for receptance output FRFs.

Figure 14 contains a receptance driving point measurement which exemplifies the symptomatic errors found by Carne and Dohrmann, that have been an occurring phenomena in the experimental stages in the making of this thesis. Motivated by the conclusions drawn from Equation (28) Carne and Dohrmann instead proposed a technique named DeCompositon Data (DCD) filtering which eliminated most of the spurious peaks from the FBS prediction.
The origin of the non-physical behaviour found in measurement data is of course of highest interest to the experimentalist. This behaviour is only attributed to either noise or subsequent mathematical prepossessing in [69]. The subject was further investigated in the context of state-space substructuring, by Sjövall and Abrahamsson in [70], and phase constrained state-space identification by McKelvey and Moheimani in [31] where non-collocated and/or non-co-oriented sensors were acknowledged as possible causes to the measurement phenomenon. A further plausible cause to the non physical behaviour can also be found in data truncation of output signals. In the article by Trethewey and Cafeo, [32], the truncation effect is studied in FRFs obtained from hammer tests.

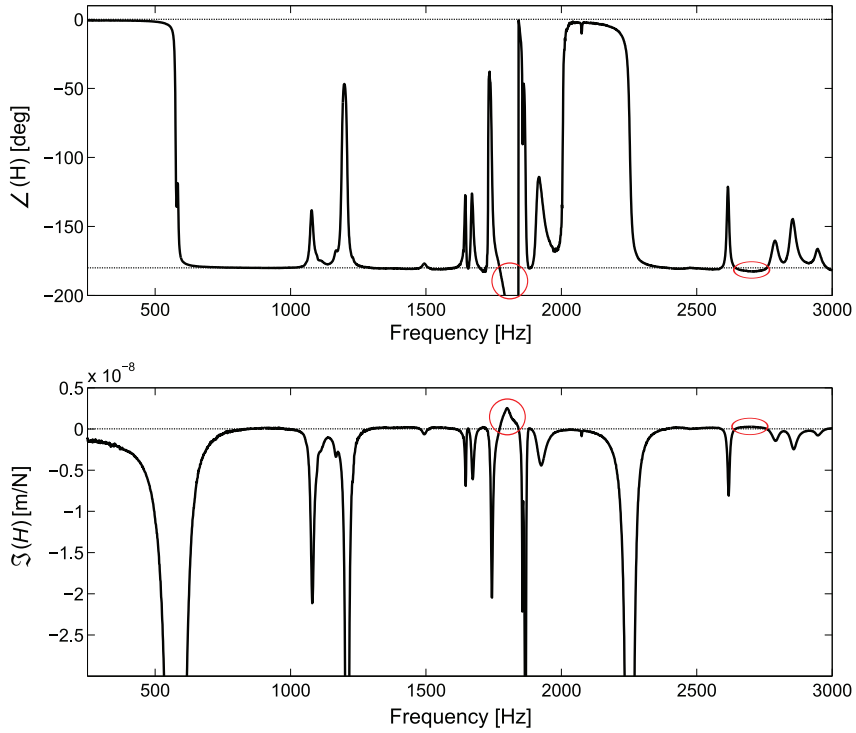

Figure 14: Example of estimated phase, $\angle$, and imaginary, $\Im$, part of drive point accelerance FRF from experimental test-rig examined in **Papers A, C** and **D**.

6.1.1 Truncation effects

A small example will be provided to illustrate the effects of output truncation that were enlightened by Trethewey and Cafeo. Considering one of the numerical structures utilized in **Paper D** for residual compensation evaluation, Figure 15, where the physical mass properties are $m_i = 1$ [kg] and stiffness, k_i, and damping, v_i, are found in Table 2.

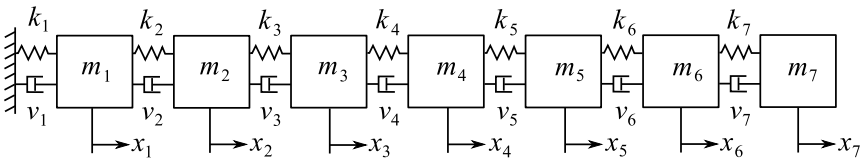

Figure 15: Numerical/experimental structure

Table 2: Physical parameter values of damping and stiffness elements

i	1	2	3	4	5	6	7
v_i [Ns/m]	110	20	70	200	300	100	50
k_i [kN/m]	253	2467	9870	19344	39478	56849	77378

By subjecting the numerical structure to the same impulse as generated in the example in section 4.2.1 at DOF 7 and calculating the response at the same manner at x_7, it can be seen that the time duration for considerable response levels is significantly longer than the duration of the force impulse, Figure 16. For lightly damped structures, the vibration response decay may be very long before the system is put to rest. This results in substantial amount of recorded data hence a truncation of the output signal is often made.

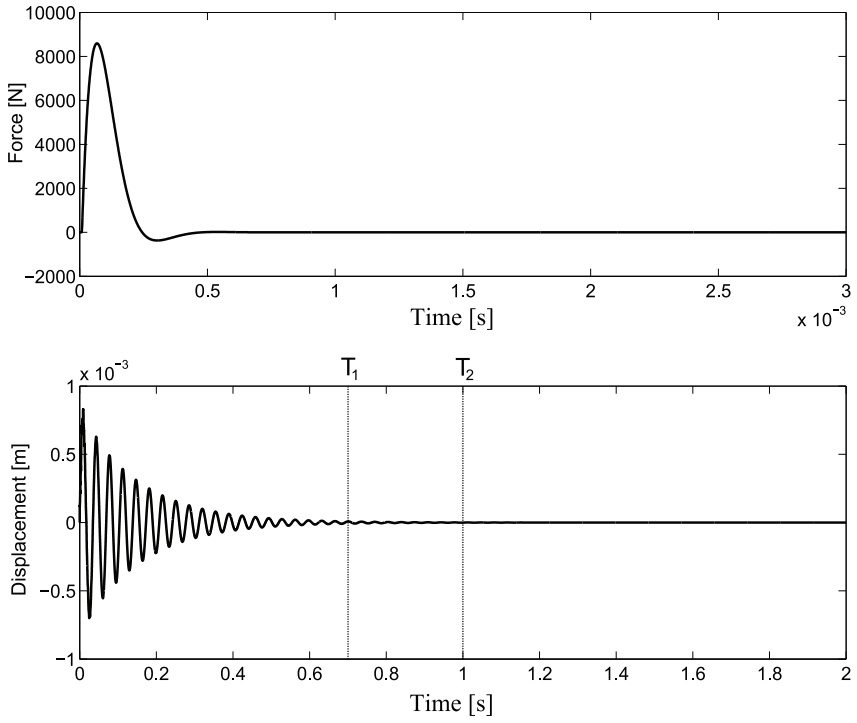

Figure 16: Impulse input and response at x_7 of numerical structure

To study the point that Trethewey and Cafeo made, the FRFs are established using `Matlab`'s `tfestimate` algorithm using two different capture times, $T_1 = 0.7$s and $T_2 = 1$s. These FRFs are compared to the theoretical FRF constructed, using Equation (22) based on the values in Table 2 using $\mathbf{M} = \mathbf{I}_{7\times 7}$ and were structure of the damping, $\mathbf{V}$ and stiffens $\mathbf{K}$ matrices are

$$\mathbf{V} = \begin{bmatrix} v_1 + v_2 & -v_2 & 0 & \cdots & 0 \\ -v_2 & \ddots & \ddots & \ddots & \vdots \\ 0 & \ddots & \ddots & & 0 \\ \vdots & \ddots & & v_6 + v_7 & -v_7 \\ 0 & \cdots & 0 & -v_7 & v_7 \end{bmatrix} \tag{29}$$

$$\mathbf{K} = \begin{bmatrix} k_1 + k_2 & -k_2 & 0 & \cdots & 0 \\ -k_2 & \ddots & \ddots & \ddots & \vdots \\ 0 & \ddots & \ddots & & 0 \\ \vdots & \ddots & & k_6 + k_7 & -k_7 \\ 0 & \cdots & 0 & -k_7 & k_7 \end{bmatrix}$$

The results are found in Figure 17, from this it is evident that the FRF established using the longer capture time is in good agreement to the true FRF. The FRF established using the shorter truncation time is however biased in both amplitude and phase. As seen the error is hard to detect in the amplitude plot without the assistance of a reference yet the phase violation is more evident. The problem can indeed be minimized using an appropriate capture time, hitting the structure multiple times or applying an exponential window on the response hereby artificially forcing a faster amplitude decay yet is an important aspect to keep track of.

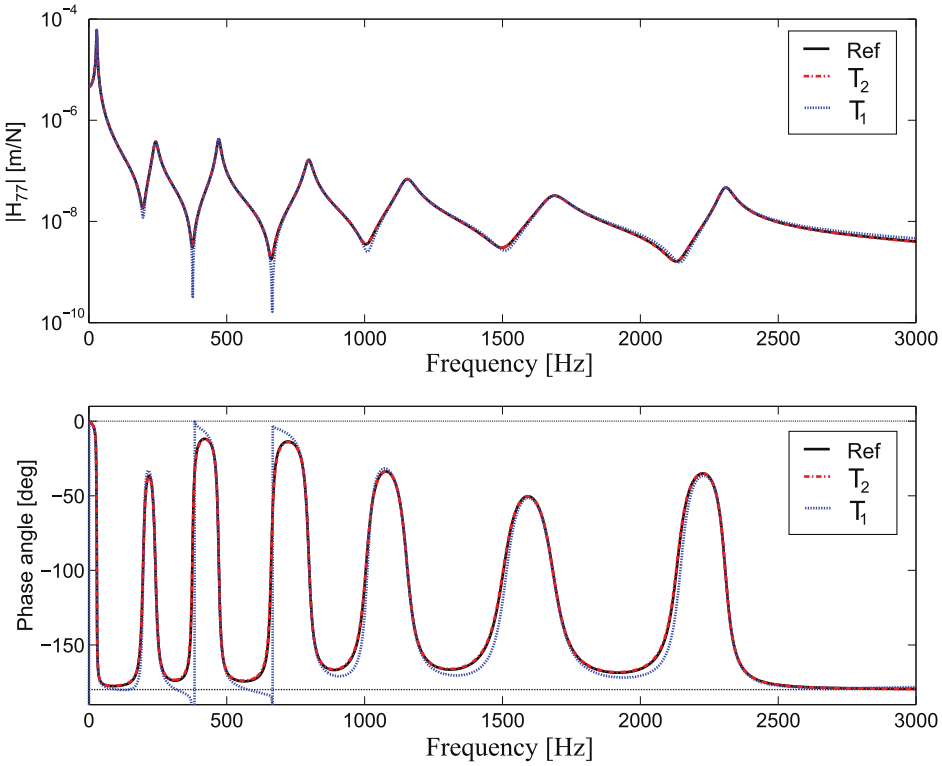

Figure 17: FRF magnitude and phase estimated with capture time T_1 and T_2 compared to theoretical reference, (Ref).

6.2 Physical model consistency

As measurement errors have been a documented problem in FBS, it may also have a devastating effect in state-space substructuring. If experimental errors occur it is highly likely that these will be adopted by the state-space model. Noise contamination has been shown to be sufficient for causing non-physical state-space model representation in Sjövall and Abrahamsson, [70]. This leads to an unstable coupled model representations as a consequence. Continuing on the example from the previous section it can be seen that the problem occurs when the FRF carries measurement anomalies that are other than noise. By subjecting the FRFs obtained using the T_1 capture time to the unconstrained state-space subspace identification algorithm `n4sid` and the LSCP algorithm, an establishment of model representations on both state-space and residue and pole form is achieved. It can be seen in Figure 18 that the model captures the FRF data very well which means that it also captures the phase violating parts. It can also be seen that the two algorithms produces identical FRFs which is not surprising since the state-space representation can be recast into residue and pole form, see **Paper C**.

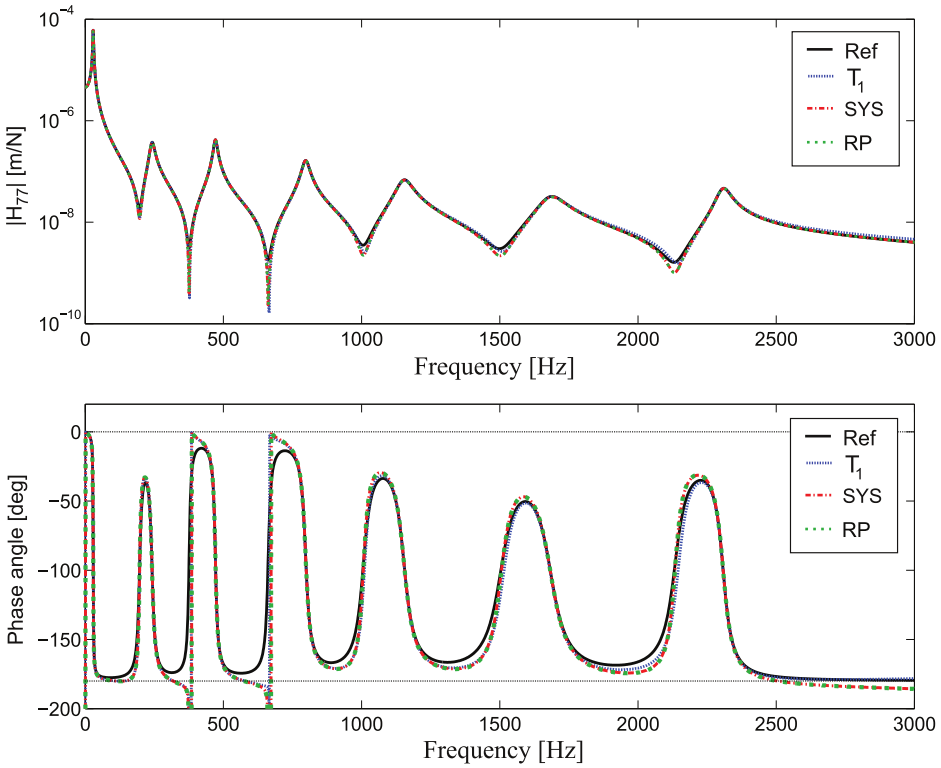

Figure 18: FRF magnitude and phase estimated with capture time T_1, identified state space models (SYS) and residue-pole model (RP), compared to the theoretical reference, (Ref).

The consequences of these measurement artifacts and the necessity to enforce *passivity* constraints on subcomponent level, preventing the model from including these measurement artifacts, are addressed in **Papers C** and **D**. By enforcing the proposed method in **Paper C** to the state-space model in the example it can be seen that the phase violation in the example is circumvented, see Figure 19.

6.3 Linear time-invariant systems

Passivity is one of the physical conditions enforced on the state-space subcomponent models in this thesis, yet others also follows based on the fundamental assumptions that the structures studied are linear time-invariant (LTI), non-gyroscopic and non-circulatory mechanical systems. Assumed as such, constraints can be placed on the structure model representation such as *causality*, *stability*, *reciprocity*, *passivity*, *displacement-velocity consistency* and *static mobility and accelerance response*. Every such constraint is not a formidable obstacle to consider during the identification pro-

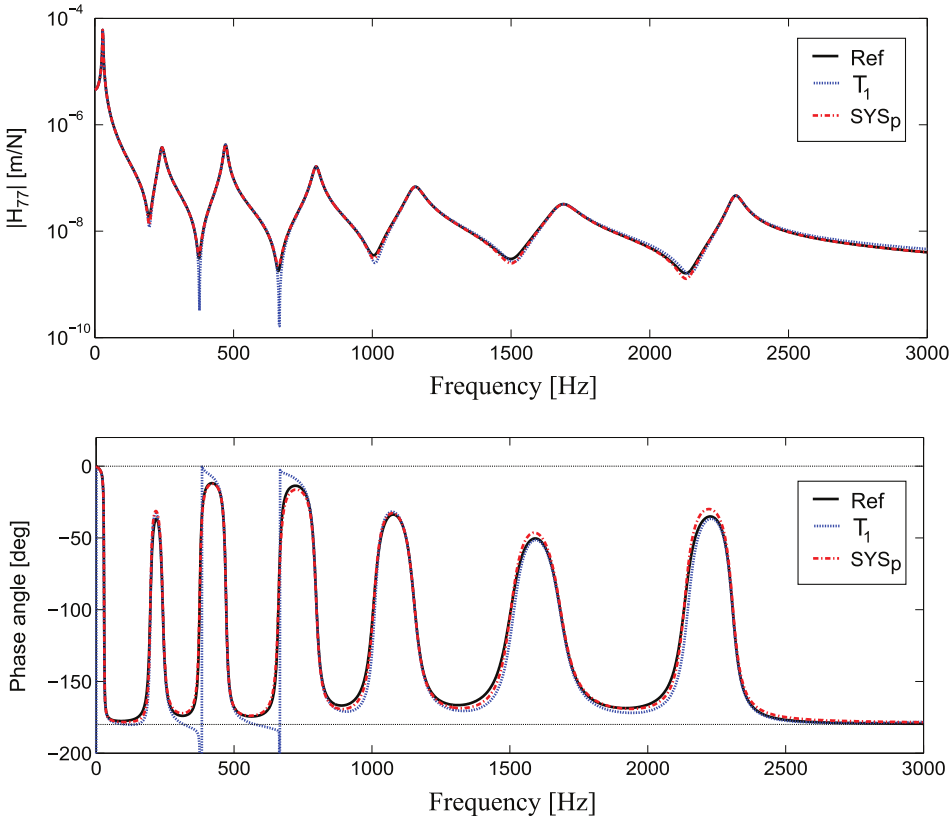

Figure 19: FRF magnitude and phase estimated with capture time T_1 enforced passivity, SYS_p, compared to the theoretical reference, (Ref).

cess but to consider them all together has been shown cumbersome, Sjövall [53]. A short description of these rules will follow:

The first rule is *causality* which is fulfilled if the system's output only depends on present and past inputs and not on future inputs. A state-space model representation as presented here, based on the real-valued quadruple, $[\mathbf{A}, \mathbf{B}, \mathbf{C}, \mathbf{D}]$, is always causal hence this property is already defined by the model structure.

Stability is another expected property for the components treated here. A time-invariant system is said to be asymptotically stable if all poles of the system matrix $\mathbf{A}$ have negative real parts. This is a property that need to be imposed to the model.

Reciprocity, is fundamental in model expansion to synthesise unmeasured inputs and outputs. Mechanical systems are expected to obey Maxwell-Betti's reciprocity principle, Meirovitch [71]. The reciprocity principle states that a system excited at location i with measured response at location j is identical to the response at i if the same

excitation force is applied at j. Hence the following mathematical relation holds

$$\mathbf{H}_{ij} = \mathbf{H}_{ji} \tag{30}$$

Passivity, much have been written within control theory about the mathematical conditions placed upon a transfer function such that it obeys the *passivity* criterion, see Bao and Lee [72]. In the context of an LTI, non-gyroscopic non-circulatory mechanical system, such as the ones studied in this thesis, the passivity criterion states that the system is passive if the total supplied power by any external loading to it, u, is positive. Further this implies that the real part of a mobility frequency transfer function is positive real for all collocated and co-oriented inputs and outputs, *i.e.* all driving point FRF elements, see [70] for proof. This is in line with the governing equations of real normal modes [36] and in analogy with this it also follows that these FRF elements are bounded within the interval of $[-90°, 90°]$. As such the state-space representation of these elements are minimum phase, [72], hence all zeros and poles are located at the negative real plane. Note that system stability does not imply passivity.

Displacement-velocity consistency, regards Newton's second law and places the restriction upon the relation between input **B** and output **C** matrices of the state-space model preventing a direct throughput term for velocity responses from applied forces. The subject is more thoroughly covered in **Paper D** but the consequence of the law is that the input and output matrices for displacement response need to fulfil the following condition **CB=0**.

The final condition regarding *static mobility and accelerance response*, is considered for mechanical structures that have no rigid body modes. The machine tool and experimental test rig, which are fixed to ground, considered in this thesis are examples of such. For these systems the velocity and accelerance response subjected to a static load is zero and a condition on their related transfer function is that $\mathbf{H}(0) = 0$. The enforcement of this constraint is provided by the formulation of passivity enforcement in **Paper C** as this property can be satisfied for all modes of the system separatly.

7 Chatter vibrations in metal cutting

Chatter vibrations can occur in all metal cutting processes and is one of the most common productivity limiting factors in metal machining. As such the ability to utilize the coupled results between the machine tool and cutting tool with respect to predictions of these vibrations is of highest priority. Comparisons between spindle speed dependant stability limit, based on FRFs obtained from state-space component synthesis and reference measurements of the fully assembled structure have been done, **Papers A, B** and **E**, to evaluate the accuracy needed in the coupling prediction. Hence a more thorough coverage of this research field will follow.

Chatter occurs from dynamic force feed-back due to variation in chip thickness during cut. The variation in chip thickness originates from a phase shift in vibration marks left on the machined surface between two consecutive cuts. This phase shift is dependent on the dynamics of the machine tool/cutting tool assembly. The spindle speed n and number of cutting teeth z govern the period time between cuts. Since the spindle speed is a process parameter to be selected by the operator, this parameter can be chosen so that the vibration marks from the previous cut is in phase with the current cut. If the vibration marks between cuts is in phase then there will be no force feed-back and there will be no regenerative vibrations. A process optimisation with support in modelling and analysis is possible provided that the vibrational properties of the tool tip is known.

7.1 Chatter in turning of a disk

The simplest explanation model of chatter vibrations in the cutting process do regard orthogonal turning of a disk where the tool is fed in the radial direction of the disk. In case of a completely stable cutting process this example would provide that the feed, f_{n}, and the uncut chip thickness h_{D}, would be the same. However, if the tool is to be considered to be flexible in the feed direction and a vibration is initiated from the entry of the cutting tool, the lamina formation of the chip or hardness variations in the work piece material can cause forced oscillations. The vibration of the cutting tool will then leave a wavy surface imprinted on the work piece. When the work piece has turned one full revolution this waveform on the surface will result in a variation in chip thickness, $h_{\mathrm{D}}(t)$, provided that there is a phase shift, ϵ, between the previous and the currently cut surface. The time dependent chip thickness, $h_{\mathrm{D}}(t)$, is in this case no longer constant with the feed per revolution f_n, of the cutting tool. The chip thickness will instead be a function of the feed per revolution f_n, the inner modulation, *i.e* current cut surface, $y(t)$ and the outer modulation, *i.e* previously cut surface, $y(t-\tau)$, see Figure 20.
The progression of the tool vibration under these conditions can take one of three forms. The first case is a stable form where the vibration is damped out over time

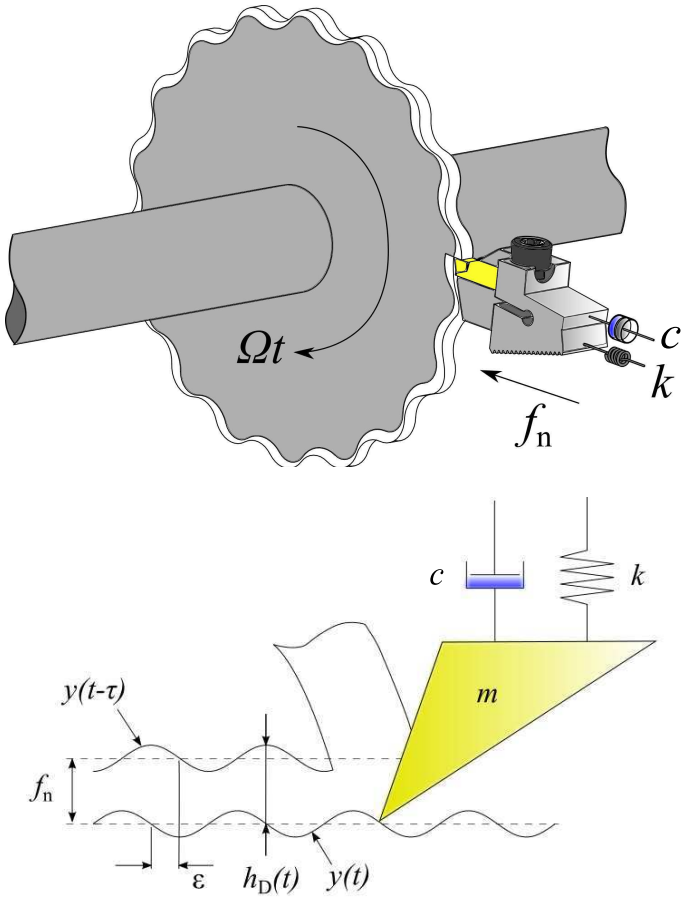

Figure 20: Chip thickness variation in a turning process subjected to regenerative vibrations.

and the vibration amplitude diminishes. The second is when the vibration stays critically stable and the vibration amplitude neither dampens out or grows and the third is when the system becomes unstable and the vibrations grow to large levels. The last case is what is known in metal machining as chatter.

7.1.1 Stability lobe diagrams in turning

The most interesting case to predict, is the case when the process is critically stable. The first researchers to work actively to predict the stability limit for the turning case were Tlustly [4] and Tobias [5]. They derived linear analytical expressions for prediction of chatter stability. They made a linearisation of the excitation force from the cutting process which permitted the stability equations to be derived in the Laplace

domain. From these an analytical expression for stability could be obtained. Both researchers stated that the cutting force acting in the feed direction, $F_{\mathrm{f}}(t)$, could be expressed as a proportional relation between the edge length in cut, a_{p}, the chip thickness, $h_{\mathrm{D}}(t)$, and the work piece material dependent specific cutting force coefficient, k_{f}, as

$$F_{\mathrm{f}}(t) = k_{\mathrm{f}} a_{\mathrm{p}} h_{\mathrm{D}}(t) \tag{31}$$

From Figure 20 it can be concluded that the variation in chip thickness can be expressed as $h_{\mathrm{D}}(t) = f_{\mathrm{n}} + y(t-\tau) - y(t)$, with τ being the time for one full turn of the work piece. Based on this conclusion the equation of motion of the system can be expressed as

$$m\ddot{y}(t) + c\dot{y}(t) + ky(t) = k_{\mathrm{f}} a_{\mathrm{p}} \left[f_{\mathrm{n}} + y(t-\tau) - y(t) \right] \tag{32}$$

The next step to derive an analytical expression for the critical stable system is to take the time invariant Delay Differential Equation (DDE) to Laplace domain. In the Laplace domain the current cut is expressed as, $Y(s) = \mathcal{L}(y(t))$ and the previous cut is expressed as $Y(s)e^{s\tau} = \mathcal{L}(y(t-\tau))$. The dynamic chip thickness in Laplace domain is therefore

$$h_D(s) = f_{\mathrm{n}} + Y(s)e^{s\tau} - Y(s) = f_{\mathrm{n}} + Y(s)(e^{s\tau} - 1) \tag{33}$$

and the dynamic cutting force in Laplace domain becomes

$$F_{\mathrm{f}}(s) = k_{\mathrm{f}} a_{\mathrm{p}} h_{\mathrm{D}}(s) \tag{34}$$

The vibration excited by the dynamic cutting force can now be written as

$$Y(s) = F_{\mathrm{f}}(s) H(s) = k_{\mathrm{f}} a_{\mathrm{p}} h_{\mathrm{D}}(s) H(s) \tag{35}$$

where $H(s) = k + sc + s^2 m$ is the transfer function between the dynamic force and the displacement. The relation between the dynamic chip thickness, $h_{\mathrm{D}}(s)$ and the feed per revolution f_{n} can, by substituting the expression of $Y(s)$ in Equation (35) into Equation (33), be expressed as

$$\frac{h(s)}{f_{\mathrm{n}}} = \frac{1}{1 + k_{\mathrm{f}} a_{\mathrm{p}} H(s)(1 - e^{s\tau})} \tag{36}$$

From Equation (36) the characteristic equation of the closed loop system is found to be

$$1 + k_{\mathrm{f}} a_{\mathrm{p}} H(s)(1 - e^{s\tau}) = 0 \tag{37}$$

The stability limit where the system is critically stable with respect to the edge length in cut, $a_{\mathrm{p}}^{\mathrm{lim}}$, can after some manipulation of Equation (37), for details see [73], be shown to be

$$a_{\mathrm{p}}^{\mathrm{lim}} = \frac{-1}{2k_{\mathrm{f}}\Re(H(s))} \tag{38}$$

Here it can be seen that only negative values of the real part of the frequency response function, $\Re(H(s))$, produces valid results since $a_{\mathrm{p}}^{\mathrm{lim}}$ has to be positive. The spindle speed and number of waves left on the work piece surface N, is related to frequency $\omega = -js$, as

$$n = \frac{\omega}{60(2\pi N + \epsilon)} \tag{39}$$

where

$$\epsilon = 3\pi + 2\psi$$

and for negative $\Re(H(s))$,

$$\psi = \begin{cases} -\pi + tan^{-1}\left|\frac{\Im H}{\Re H}\right| & \text{if } \Im H < 0 \\ -\pi - tan^{-1}\left|\frac{\Im H}{\Re H}\right| & \text{if } \Im H > 0 \end{cases}$$

Figure 21 shows how the solution of Equation (38) corresponds to the stability limit of the first stability lobe, *i.e.* $N = 0$.
A stability lobe diagram for a specified spindle speed interval can now be created by solving Equations (38)-(39) for a sufficient number of lobes N, see Figure 22.
From Figure 22 it can be seen that some spindle speeds are better than others where larger edge lengths in cut, a_{p}, can be machined without encountering chatter. It can also be seen that for higher numbers of surface waves the closer the lobes get and the lesser the stability boundary for edge length in cut $a_{\mathrm{p}}^{\mathrm{lim}}$ varies with spindle speed.

7.2 Chatter in milling

Turning is usually a slow cutting process with a high tool tip resonance frequency which means that the number of vibration cycles during a full turn is large. This means that optimising a turning process with respect to chatter often given little room for improvement. The milling process is more prone to improvements from spindle speed optimisation and especially in the high speed machining segments. The main reason that the milling process can draw greater advantage from the stability optimisation is that the phase between the inner and outer surface modulations from one material removal cut is generated by two cutting teeth. Most of the commercial milling cutters have more that one cutting tooth resulting in a tooth passing frequency which is higher than the spindle revolution frequency. As a result of this, in combination

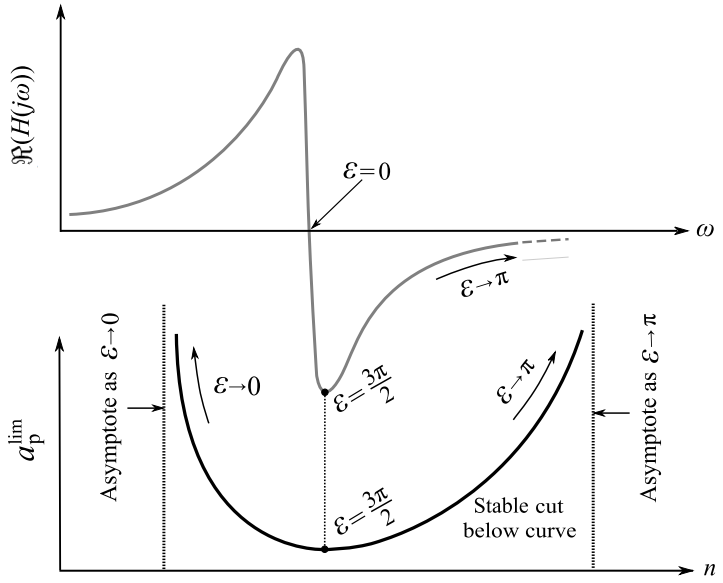

Figure 21: Relation between real part FRF $\Re(H(j\omega)$ and stability lobe for $N = 0$

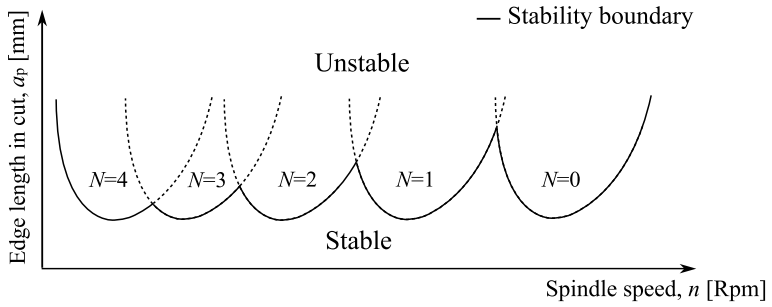

Figure 22: Stability lobe diagram

with a more flexible cutting tool with lower resonance frequencies, a lower number of vibration waves N needs to be considered for normal spindle speeds. This results in larger and wider stability lobes. The difference between ”good” and ”bad” spindle speeds is therefore larger in terms of stable cutting edge length in cut a_{p}, or axial depth of cut which is the proper term in milling.

7.2.1 Stability lobe diagrams in milling

The chatter phenomenon in milling has many similarities to the related phenomenon in turning but there are some differences, both in terms of chatter mechanics and stability theory. The most significant difference between milling and turning is that

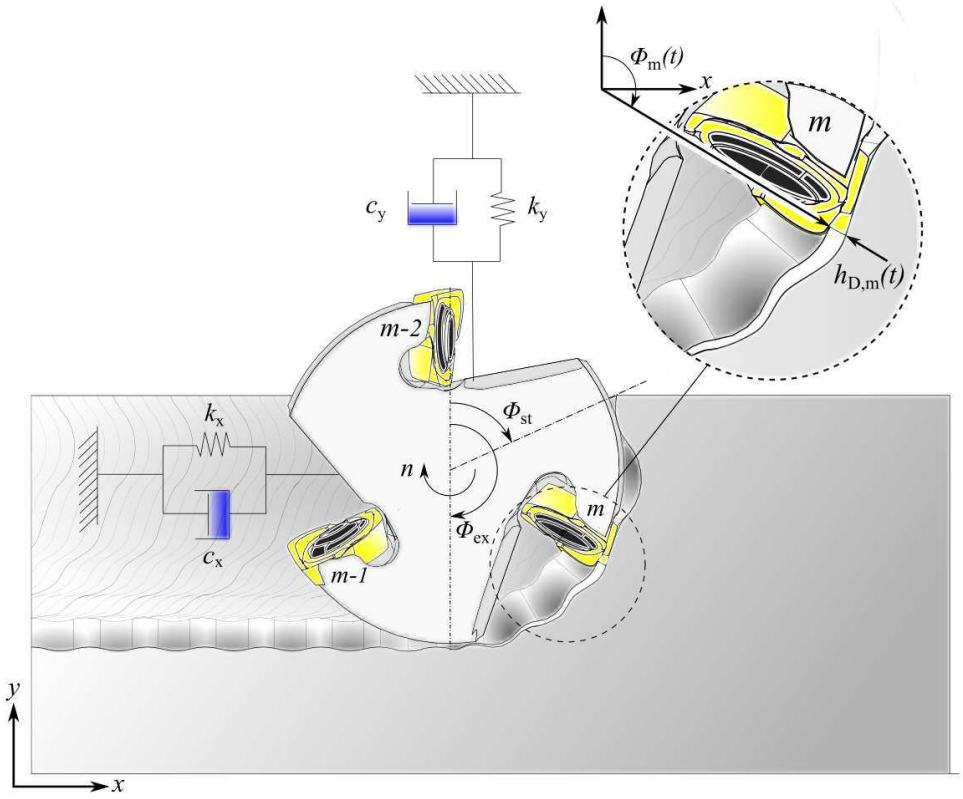

Figure 23: Illustration of a 2-DOF dynamic milling model considering transversal motion in two directions. The figure defines the entering angle ϕ_{st}, and exiting angle ϕ_{ex} in relation to the cutter and work piece. The dynamic chip thickness $h_{\mathrm{D,m}}(t)$, is defined as the relation between the angle in cut ϕ_{m}, of tooth m and the dynamic displacement between the two consecutive teeth $m-1$ and m.

in the milling process the cutting tool is rotating and not the work piece as it is in turning. This makes the theoretical assessment of stability lobe analysis somewhat more cumbersome, since the cutting forces change both direction and amplitude during the cut. This is due to the change in orientation of the cutting tooth and variation in chip thickness, see Figure 23.

An analytical method to get the chatter stability diagram in milling was first derived by Budak and Altintas [6, 7] who proposed a similar linearisation approach to the cutting force model as described in [4] and [5]. However, they included both the tangential and radial cutting forces, $F_{\mathrm{t,m}}$ and $F_{\mathrm{r,m}}$, acting on the cutting tooth during cut.

For the m:th tooth we have

$$F_{\mathrm{t,m}}(t) = k_{\mathrm{t}} a_{\mathrm{p}} h_{\mathrm{m}}(t) \tag{40}$$

$$F_{\mathrm{r,m}}(t) = k_{\mathrm{r}} a_{\mathrm{p}} h_{\mathrm{m}}(t) \tag{41}$$

The angle dependent chip thickness $h_{\mathrm{D,m}}(t)$, see Figure 23, can be approximated as

$$h_{\mathrm{D,m}}(t) = \begin{cases} f_{\mathrm{z}} \sin\phi_{\mathrm{m}}(t) + (\upsilon_{\mathrm{m\text{-}1}} - \upsilon_{\mathrm{m}}), & \phi_{\mathrm{st}} < \phi_{\mathrm{m}} < \phi_{\mathrm{ex}} \\ 0, & \phi_{\mathrm{ex}} < \phi_{\mathrm{m}} < \phi_{\mathrm{st}} \end{cases} \tag{42}$$

where $f_{\mathrm{z}} \sin\phi_{\mathrm{m}}(t)$ is the static chip thickness and υ_{m} and $\upsilon_{\mathrm{m\text{-}1}}$ is the dynamic displacements in radial direction of the m:th and $(m-1)$:th cutting teeth. Equation (42) can be expressed as a function of the tooth passing period τ, see Figure 24, as

$$h_{\mathrm{D,m}}(t) = \begin{cases} f_{\mathrm{z}} \sin\phi_{\mathrm{m}}(t) + (\upsilon(t) - \upsilon(t-\tau)), & \phi_{\mathrm{st}} < \phi_{\mathrm{m}} < \phi_{\mathrm{ex}} \\ 0, & \phi_{\mathrm{ex}} < \phi_{\mathrm{m}} < \phi_{\mathrm{st}} \end{cases} \tag{43}$$

With the assumption that there is no coupling between the radial and tangential degrees of freedom the total force contribution from all cutting edges z, can be written

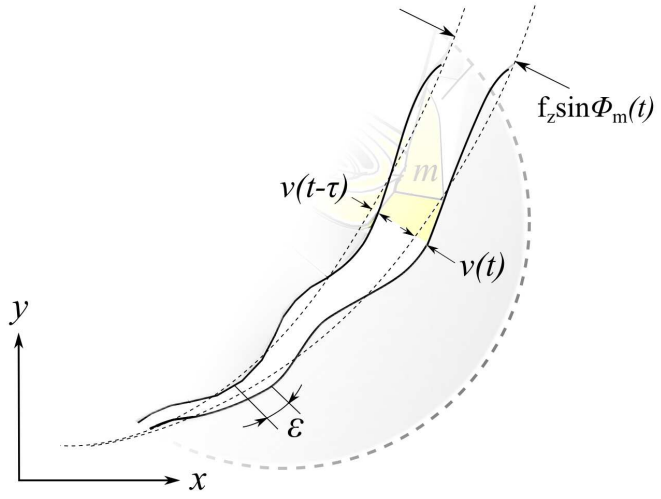

Figure 24: Illustration of the dynamic chip thickness in milling as a function of the static feed dependent chip thickness $f_{\mathrm{z}} \sin\phi_{\mathrm{m}}(t)$. Here f_{z} is the feed per tooth and ϕ_{m} is the angle in cut. It is also a function of the phase shift ϵ, which depend on the dynamic radial displacements $\upsilon(t)$ and $\upsilon(t-\tau)$.

as

$$F_{\mathrm{x}}(t) = -\sum_{m=0}^{z-1} F_{\mathrm{t,m}}(t)\cos\phi_{\mathrm{m}}(t) - \sum_{m=0}^{z-1} F_{\mathrm{r,m}}(t)\sin\phi_{\mathrm{m}}(t) \tag{44}$$

$$F_{\mathrm{y}}(t) = \sum_{m=0}^{z-1} F_{\mathrm{t,m}}(t)\sin\phi_{\mathrm{m}}(t) - \sum_{m=0}^{z-1} F_{\mathrm{r,m}}(t)\cos\phi_{\mathrm{m}}(t) \tag{45}$$

Here, the tangential and radial cutting forces have been projected to the table fixed coordinate system xy, see Figure 23.

Equations (44) and (45) were used in [6] and [7] to derive equations (46) and (47) as the foundation for the analytical stability lobe diagram of a milling process. These are for the axial depth of cut

$$a_{\mathrm{p}}^{\mathrm{lim}} = -\frac{2\pi\Re(\lambda)}{zk_{\mathrm{t}}}(1-\kappa) \tag{46}$$

where λ and κ can be found from

$$\lambda = -\frac{1}{2\alpha_0}\alpha_1 \pm \sqrt{\alpha_1 - 4\alpha_0}$$

with

$$\alpha_0 = H_{\mathrm{xx}}(j\omega)\,H_{\mathrm{yy}}(j\omega)\,(\alpha_{\mathrm{xx}}\alpha_{\mathrm{yy}} - \alpha_{\mathrm{xy}}\alpha_{\mathrm{yx}})$$

$$H_{\mathrm{xx}}(j\omega) = \frac{1}{-\omega^2 M + j\omega c_x + k_x}$$

$$H_{\mathrm{yy}}(j\omega) = \frac{1}{-\omega^2 M + j\omega c_y + k_y}$$

$$\alpha_1 = \alpha_{\mathrm{xx}}H_{\mathrm{xx}}(j\omega) + \alpha_{\mathrm{yy}}H_{\mathrm{yy}}(j\omega)$$

$$\alpha_{\mathrm{xx}} = \frac{1}{2}\left[\cos 2\phi - 2\frac{k_{\mathrm{r}}}{k_{\mathrm{t}}}\phi + \frac{k_{\mathrm{r}}}{k_{\mathrm{t}}}\sin 2\phi\right]_{\phi_{\mathrm{st}}}^{\phi_{\mathrm{ex}}}$$

$$\alpha_{\mathrm{xy}} = \frac{1}{2}\left[-\sin 2\phi - 2\phi + \frac{k_{\mathrm{r}}}{k_{\mathrm{t}}}\cos 2\phi\right]_{\phi_{\mathrm{st}}}^{\phi_{\mathrm{ex}}}$$

$$\alpha_{\mathrm{yx}} = \frac{1}{2}\left[-\sin 2\phi + 2\phi + \frac{k_{\mathrm{r}}}{k_{\mathrm{t}}}\cos 2\phi\right]_{\phi_{\mathrm{st}}}^{\phi_{\mathrm{ex}}}$$

$$\alpha_{\mathrm{yy}} = \frac{1}{2}\left[-\cos 2\phi - 2\frac{k_{\mathrm{r}}}{k_{\mathrm{t}}}\phi - \frac{k_{\mathrm{r}}}{k_{\mathrm{t}}}\sin 2\phi\right]_{\phi_{\mathrm{st}}}^{\phi_{\mathrm{ex}}}$$

$$\kappa = \frac{\Im(\lambda)}{\Re(\lambda)}$$

and the corresponding spindle speed is

$$n = \frac{60\omega}{z\left(\epsilon + 2\pi N\right)} \tag{47}$$

where the phase angle ϵ is

$$\epsilon = \pi - 2\psi$$

and

$$\psi = \begin{cases} -tan^{-1}\left|\frac{\Im H(j\omega)}{\Re H(j\omega)}\right| & \text{if } \Re H(j\omega) > 0,\ \Im H(j\omega) < 0 \\ -\pi + tan^{-1}\left|\frac{\Im H(j\omega)}{\Re H(j\omega)}\right| & \text{if } \Re H(j\omega) < 0,\ \Im H(j\omega) < 0 \\ -\pi - tan^{-1}\left|\frac{\Im H(j\omega)}{\Re H(j\omega)}\right| & \text{if } \Re H(j\omega) < 0,\ \Im H(j\omega) > 0 \\ -2\pi + tan^{-1}\left|\frac{\Im H(j\omega)}{\Re H(j\omega)}\right| & \text{if } \Re H(j\omega) > 0,\ \Im H(j\omega) > 0 \end{cases}$$

Since the overall objective with the substructuring approach taken to the machine tool/cutting tool assembly is for process stability analysis the presented analytical expression for the stability lobes have been utilized for evaluation purposes in **Papers A, B** and **E**.

7.3 Time domain chatter stability boundary

The analytical chatter stability methods for obtaining stability lobe charts have both advantages and disadvantages. One great advantage is that the analytical methods are fast. The two main phenomena the analytical methods does not consider are when the cutting tooth jumps out of the work piece due to excessive vibrations, and when the cutting force is strongly non-linearly related to feed or cutting speed. In these cases time domain simulations produce better results. The time domain simulation approach to predict chatter has been utilised by a number of researchers, see [8–17]. The two most commonly used methods for time domain chatter stability predictions are the Temporal Finite Element Analysis (TFEA) method, see [8, 9], and the Semi-Discretisation (SD) method, see [10–13].

The TFEA method compares the exact analytical solution for free tool vibration with an approximated solution of the tool vibrations during cut. The time-delay differential equation has no closed form solution for the milling process so an approximated solution of the tool in cut is therefore established by dividing the time in cut into finite numbers of time segments for the comparison. The two systems are then compared in a discrete linear map where the stability is determined by the characteristic multiplier of the map.

The SD method has been employed to approximate the delay differential equations (DDE) describing the stability of milling and turning operations by a series of ordinary differential equations (ODE). This is archived by approximating the time delay terms as piecewise constant functions.

The TFEA and SD methods have both been employed to predict stability lobe charts for a low radial immersion SDOF milling operation by Bayly *et al.* and Insperger *et al.* see [8] and [10]. Both methods were later extended to a more general 2 DOF milling operation by Mann *et al.* [9] who used TFEA and Gradišek [14] who used the SD method. The various time domain methods, see [8–17], all differ from the analytical methods in that they have to be solved iteratively in order to find the stability boundary of the axial depth of cut $a_{\mathrm{p}}^{\mathrm{lim}}$. Common to all investigations presented in [8–17], is also that they all search for the bifurcation point, *i.e.* the limiting depth of cut were the system becomes unstable. Different bifurcation types have been found to occur with Hopf-bifurcation being the most common type. This usually manifests itself as a chatter frequency close to a natural frequency of the system, see [11]. The second bifurcation type observed using the TFEA method or the SD method is flip-bifurcation which is characterised by a chatter frequency at harmonics of odd multiples of half the tooth passing frequency, see [14]. The time-domain solutions of milling and turning provides more information regarding the cutting process than the analytical methods. The time-domain simulation approach to the metal cutting process can be extended not only to determine chatter but also to quantify the severity of the vibrations and be used to predict surface texture during stable and unstable conditions, see [74].

8 Summary of appended papers

Paper A: *Dynamic substructuring in metal cutting machine chatter*

The RDOF using a single experimental set-up is addressed using system identification and model expansion taking the conceptual approach of experimental dynamic testing and system identification on state space form. The experimental set-up was applied to a physical test rig. The state-space coupling algorithms were employed to couple the identified test rig structure to a synthesised subsystem representing the cutting tool. The model of the cutting tool was based on the mass and inertia properties retrieved from a CAD model tool. The experimental set-up combined with system identification and model expansion allowed for the experimentally obtained system model and the assembled structure model to contain a five degree of freedom model representation. This was an expansion of the frequency response function matrix describing the coupled system to include also cross FRF relations between the five DOFs which was novel at the time. The synthesised FRFs of the assembled substructures were compared and evaluated against measurements of the fully assembled test rig with encouraging yet not fully satisfactory results.

Paper B: *Experimental-analytical substructure model sensitivity analysis for cutting machine chatter prediction*

A sensitivity analysis of parameter influence on the coupled system was conducted. A number of parameters related to the identification process were perturbed in order to see the magnitude of influence each parameter had on the coupled system. The effect of perturbation of parameters such as state-order, FRF response magnitude, damping estimation and frequency cut-off were investigated. A reference system was constructed based on an FE model of the test rig used in **Paper A** and the parameter influence investigation was conduced based on perturbations of the reference system. Concluded from the output of the study is that an appropriate state order is of the essence in model based substructuring. A more general conclusion applied to all coupling methods is that the amplitude of the frequency response functions strongly influences the coupled results hence puts high demands on the experimental accuracy and sensor calibration.

Paper C: *Dynamic sub-structuring with passive state-space components*

Unstable poles found in the coupled system models are addressed. The problem is found in coupled system model presented in **Paper A** in which one of the system models is obtained based on experimental dynamic testing and system identification. The problem could not be observed in **Paper B** where both subcomponents originates from physically consistent FE data. The problem hinders time domain simulations of the coupled results and the problem was found to originate from passivity violations of the experimentally obtained state-space models. The paper addresses this issue and presents a novel method to enforce *passivity* and *static mobility response* stationarity for constrained MIMO mobility FRFs resulting in state space subsystem models taken to a driving point minimum phase state, hereby assuring model stability leading to numerical stability.

Paper D: *Residual compensation in experimental state space model synthesis*

The modal incompleteness aspect of identified state-space models is taken into consideration. The modal contribution of modes outside the measured frequency interval influences the coupled results and compensation strategies can be found on other system model descriptions but not for a state-space formulation. A developed method to account for both high and low frequency residuals of state space models is presented and integrated in the overall coupling strategy that assures physical consistency of the coupled state-space models. The results are evaluated on both numerical and experimental data showing improvements on coupled results against reference models and measurements. An interesting finding presented is that modal incompleteness may lead to passivity violation.

Paper E: *On rotational degrees of freedom for substructure synthesis of machine tool and cutting tools*

The developed experimental test and coupling strategy as presented in, **Papers A-D**, is finally evaluated on a physical machine tool. The paper emphasis is on the evaluation of the most suitable experimental and theoretical method to synthesize rotational degrees of freedom. The methods proposed by [20] and [22] are compared to the developed coupling method. It lifts overlooked erroneous phenomenons, symptomatic to each investigated strategy, occurring in the synthesised RDOF FRFs and presents probable causes and the effect these have on the coupled system. The evaluation is performed on both analytical and experimental structures.

9 Conclusions and future work

A method for component synthesis of machine tool and cutting tool assemblies based on experimentally and numerically obtained state-space subcomponents has been presented. The emphasis has been on robustness and generality of the coupling procedure and lifts and addresses challenging aspects originating from both the experimental and modelling sides. The robustness aspects lies in the ability to assure a model description on coupled form that is fit for further analysis and holds the properties expected from a general LTI, non-gyroscopic, non-circulatory stable system. The developed methodology is hereby not solely devoted to machine tool structures.

It has been experienced that the truly challenging aspect of experimental dynamic substructuring that effects the accuracy the most is in the experimental part. The proposed method has been shown to sufficiently assist in metal cutting stability predictions, however, the inability to properly measure the rotational degrees of freedom, response errors inherited by signal processing, placement and calibration errors of sensors and so on, all contribute to uncertainties of the magnitude that may easily overshadow the predicted results. The proposed method constrains the substructure model description from violation of well defined physical principles, and was found to fundamentally influence the state-space coupling results. This makes the coupled results more robust, yet it will never fully compensate for poor measurement results.

A compensation method for mode contributions outside the measured frequency range have been addressed. The methodology has further been successfully implemented in the overall methodology to assure a physically consistent state-space coupled result. The taken approach has been shown to improve the prediction of eigenvalue and antiresonance locations still maintaining a stable and passive coupled state-space model.

Expansion strategies to establish unmeasured FRF elements in both frequency domain and on state-space model form have been a subject of investigation. The differences these strategies impose have been evaluated on both subcomponent level and on coupled form. From this evaluation it can be concluded that the generation of RDOFs in the frequency domain by decoupling is extraordinary sensitive to model and experimental errors.

The overall objective to, develop a robust experimentally based coupling approach to synthesise machine tool and cutting tool structures has been met. However, improvement potential can be identified on a number of accounts. From the experimental evaluation regarding the residual compensation strategy, presented in **Paper D**, a better strategy to find the optimal number and location of the compensational poles should be made instead of the ad hoc method used in the paper. Such approach would further be of interest for the identified shortcoming in **Paper E** where it was found that the placement of moment to rotational response antiresonances are governed by the location of the compensational modes.

References

[1] T. Surmann and D. Enk. Simulation of milling tool vibration trajectories along changing engagement conditions. *International Journal of Machine Tools and Manufacture*, 47(9):1442–1448, 2007.

[2] T. Surmann and D. Biermann. The effect of tool vibrations on the flank surface created by peripheral milling. *CIRP Annals - Manufacturing Technology*, 57(1):375–378, 2008.

[3] C. Eksioglu, Z.M. Kilic, and Y. Altintas. Discrete-time prediction of chatter stability, cutting forces, and surface location errors in flexible milling systems. *Journal of Manufacturing Science and Engineering*, 134(6), 2012.

[4] J. Tlustly and M. Polacek. The stability of machine tools against self excided vibrations in machining. *International Research in Production Engineering*, ASME:465–474, 1963.

[5] S.A. Tobias. *Machine Tool Vibrations*. Blackie and Sons Ltd., 1965.

[6] E. Budak and Y. Altintas. Analytical prediction of chatter stability in milling—part i: General formulation. *Journal of Dynamic Systems, Measurement, and Control*, 120(1):22–30, 1998.

[7] E. Budak and Y. Altintas. Analytical prediction of chatter stability in milling—part ii: Application of the general formulation to common milling systems. *Journal of Dynamic Systems, Measurement, and Control*, 120(1):31–36, 1998.

[8] P.V. Bayly, B.P. Mann, T.L. Schmitz, D.A. Peters, S. Gabor and T. Insperger. Effects of radial immersion and cutting direction on chatter instability in end-milling. In *Proceedings of IMECE 2002, ASME International Mechanical Engineering Congress and Exposition, New Orleans, Louisiana*, 2002.

[9] B.P. Mann, P.V. Bayly, M.A. Davies, and J.E. Halley. Limit cycles, bifurcations, and accuracy of the milling process. *Journal of Sound and Vibration*, 277(1-2):31 – 48, 2004.

[10] T. Insperger, B.P. Mann, G. Stépán, and P.V. Bayly. Stability of up-milling and down-milling, part 1: alternative analytical methods. *International Journal of Machine Tools and Manufacture*, 43(1):25 – 34, 2003.

[11] T. Kalmár-Nagy, S. Gábor, and F. Moon. Subcritical hopf bifurcation in the delay equation model for machine tool vibrations. *Nonlinear Dynamics*, 26:121–142, 2001.

[12] T. Insperger, D.A.W. Barton, and G. Stépán. Criticality of hopf bifurcation in state-dependent delay model of turning processes. *International Journal of Non-Linear Mechanics*, 43(2):140 – 149, 2008.

[13] T. Insperger and G. Stépán. Chatter suppression of turning process via periodic modulation of the spindle speed - a 1 dof analysis. In *Proceedings of the Third Conference on Mechanical Engineering, Budapest, Hungary*, 2002.

[14] J. Gradišek, M. Kalveram, T. Insperger, K. Weinert, G. Stépán, E. Govekar, and I. Grabec. On stability prediction for milling. *International Journal of Machine Tools and Manufacture*, 45(7–8):769 – 781, 2005.

[15] M.X. Zhao and B. Balachandran. Dynamics and stability of milling process. *International Journal of Solids and Structures*, 38(10-13):2233 – 2248, 2001.

[16] J. Gradišek, E. Govkar, and I. Grabec. Chatter onset in non-regenerative cutting: A numerical study. *Journal of Sound and Vibration*, 242(5):829 – 838, 2001.

[17] A. Ganguli. *Chatter reduction through active vibration damping*. PhD thesis, Université Libre De Bruxelles, Bruxelles, Belgium, 2005.

[18] T.L. Schmitz and R.R. Donalson. Predicting high-speed machining dynamics by substructure analysis. *CIRP Annals - Manufacturing Technology*, 49(1):303 – 308, 2000.

[19] T.L. Schmitz, Matthew A.D., and Michael D.K. Tool point frequency response prediction for high-speed machining by RCSA. *Journal of Manufacturing Science and Engineering*, 123(4):700–707, 2001.

[20] S.S. Park, Y. Altintas, and M. Movahhedy. Receptance coupling for end mills. *International Journal of Machine Tools and Manufacture*, 43(9):889 – 896, 2003.

[21] T. Schmitz. Receptance coupling for high-speed machining dynamics prediction. *Proceedings of the 21st International Modal Analysis Conference*, pages 1–12, 2003.

[22] T.L. Schmitz and G.S. Duncan. Three-Component Receptance Coupling Substructure Analysis for Tool Point Dynamics Prediction. *Journal of Manufacturing Science and Engineering*, 127(4):781, 2005.

[23] A. Erturk, H. Ozguven, and E. Budak. Analytical modeling of spindle – tool dynamics on machine tools using Timoshenko beam model and receptance coupling for the prediction of tool point FRF. *International Journal of Machine Tools and Manufacture*, 46(15):1901–1912, 2006.

[24] T. Schmitz and G. Duncan. Receptance coupling for dynamics prediction of assemblies with coincident neutral axes. *Journal of Sound and Vibration*, 289(4-5):1045–1065, 2006.

[25] S.S. Park and J. Chae. Joint identification of modular tools using a novel receptance coupling method. *The International Journal of Advanced Manufacturing Technology*, 35(11-12):1251–1262, 2008.

[26] I. Mancisidor, M. Zatarain, J. Muñoa, and Z. Dombovari. Fixed Boundaries Receptance Coupling Substructure Analysis for Tool Point Dynamics Prediction. *Advanced Materials Research*, 223:622–631, 2011.

[27] B. Jetmundsen, R. L. Bielawa and W.G. Flannelly. Generalized frequency domain substructure synthesis. *Journal of the American Helicopter Society*, 33(1):55–64, 1988.

[28] D.J. Ewins. *Modal Testing: Theory, Practice and Application*. Research studies press LDT., 2001.

[29] M.L.M Duarte. *Experimentally-derived structural models for use in further dynamic analysis*. PhD thesis, University of London London, 1996.

[30] T. Lim. A Theoretical and Computational Study of the FRF-Based Substructuring Technique Applying Enhanced Least Square and Tsvd
Approaches. *Journal of Sound and Vibration*, 231(4):1135–1157, 2000.

[31] T. McKelvey and S.O.R. Moheimani. Estimation of phase constrained MIMO transfer functions with application to flexible structures with mixed collocated and non-collocated actuators and sensors. In *World Congress*, volume 16, pages 36–36, 2005.

[32] M.W. Trethewey and J.A. Cafeo. Tutorial: signal processing aspects of structural impact testing. *The International Journal of Analytical and Experimental Modal Analysis*, 7(2):129–149, 1992.

[33] S. Timoshenko, D.H. Young, and W. Weaver. *Vibration Problems in Engineering*, volume 208. John Wiley and Sons, Inc., 1990.

[34] V. Koloušek, R.F. McLean, and J.S. Fleming. *Dynamics in engineering structures*. Butterworths, London, 1973.

[35] N. Saabye and H. Petersson. *Introduction to the Finite Element Method*. Prentice Hall Internationa, 1992.

[36] R.R. Craig and A.J. Kurdila. *Fundamentals of Structural Dynamics*. Wiley, 2006.

[37] W.K. Gawronski. *Dynamics and control of structures: a modal approach*. Springer, New York, 1998.

[38] M.I. Friswell, J.E. Mottershead, SpringerLink (Online service), and SpringerLink Archive (e-book collection). *Finite Element Model Updating in Structural Dynamics*, volume 38. Springer Netherlands, Dordrecht, 1995.

[39] L. Ljung. *System Identification: Theory for the User (2nd Edition)*. Prentice Hall PTR, 1998.

[40] P. Overschee, B. Moor, SpringerLink (Online service), and SpringerLink Archive (e-book collection). *Subspace Identification for Linear Systems: Theory - Implementation - Applications*. Springer US, Boston, MA, 1996.

[41] A. Brandt. *Noise and vibration analysis: signal analysis and experimental procedures*. Wiley, Chichester; Hoboken, N.J, 2011.

[42] N.M.M. Maia. *Extraction of Valid Modal Properties from Measured Data in Structural Vibrations*. University of London, 1988.

[43] T. McKelvey, H. Akcay, and L. Ljung. Subspace-based multivariable system identification from frequency response data. *IEEE Transactions on Automatic Control*, 41(7):960–979, 1996.

[44] V. Yaghoubi and T. Abrahamsson. Automated modal analysis based on frequency response function estimates. In R. Allemang, J. De Clerck, C. Niezrecki, and J.R. Blough, editors, *Topics in Modal Analysis I, Volume 5*, Conference Proceedings of the Society for Experimental Mechanics Series, pages 9–18. Springer New York, 2012.

[45] W.C. Hurty. Dynamic analysis of structural systems using component modes. *AIAA Journal*, 3(4):678–685, 1965.

[46] R.R. Craig, Jr. and M.C.C. Bampton. Coupling of substructures for dynamic analysis. *AIAA Journal*, 6(7):1313–1319, 1968.

[47] R.R. Craig, Jr. and M.C.C. Bampton. On the use of attachment modes in substructure coupling for dynamic analysis. In *AIAA/ASME 18th Structures, Structural Dynamics and Materials Conference, San Diego, CA*, 1977.

[48] D.J. Rixen. A dual Craig-Bampton method for dynamic substructuring. *Journal of Computational and Applied Mathematics*, 168(1-2):383–391, 2004.

[49] D.D. Klerk, D.J. Rixen, and S.N. Voormeeren. General framework for dynamic substructuring: History, review and classification of techniques. *AIAA Journal*, 46(5):1169–1181, 2008.

[50] R.E.D. Bishop and D.C. Johnson. *The mechanics of vibration*. Cambridge University Press, Cambridge, 1960.

[51] Y. Ren and C.F. Beards. On substructure synthesis with frf data. *Journal of Sound and Vibration*, 185(5):845–866, 1995.

[52] B. Jetmundsen. *On frequency domain methodologies for prescribed structural modification and subsustem sysnthesis*. PhD thesis, Rensselaer Polytechnic Institute, Troy, New York, 1986.

[53] P. Sjövall. *Identification and Synthesis of Components for Vibration Transfer Path Analysis*. PhD thesis, Chalmers University of Technology, Gothenburg, Sweden, 2007.

[54] T.J. Su and J.N. Juang. Substructure system identification and synthesis. *Journal of Guidance, Control and Dynamics*, 17(5):1087–1095, 1994.

[55] M. Namazi, Y. Altintas, T. Abe, and N. Rajapakse. Modeling and identification of tool holder—spindle interface dynamics. *International Journal of Machine Tools and Manufacture*, 47(9):1333 – 1341, 2007.

[56] E.B. Kivanc and E. Budak. Structural modeling of end mills for form error and stability analysis. *International Journal of Machine Tools and Manufacture*, 44(11):1151 – 1161, 2004.

[57] I. Mancisidor, A. Urkiola, R. Barcena, J. Munoa, Z. Dombovari, and Mikel Zatarain. Receptance coupling for tool point dynamic prediction by fixed boundaries approach. *International Journal of Machine Tools and Manufacture*, 78:18 – 29, 2014.

[58] K. Ahlin, M. Magnevall, and A. Josefsson. Simulation of forced response in linear and nonlinear mechanical systems using digital filters. In *International Conference on Noise and Vibration Engineering (ISMA2006)*. Katholieke univ. Leuven, Dept. Werktuigkunde, 2006.

[59] P. Welch. The use of fast fourier transform for the estimation of power spectra: A method based on time averaging over short, modified periodograms. *IEEE Transactions on Audio and Electroacoustics*, 15(2):70–73, 1967.

[60] M. Imregun, D.A. Robb, and D.J. Ewins. Structural Modification and Coupling Dynamic Analysis Using Measured FRF Data, In *5th International Modal Analysis Conference* IMAC V, London, 1987.

[61] D.J. Ewins and P.T. Gleeson. Experimental determination of multidirectional mobility data for beams. *Shock and Vibration Bulletin*, 5:153–173, 1975.

[62] W. Liu and D. Ewins. The importance assessment of rdof in frf coupling analysis. In *Proceedings of the Seventeenth International Modal Analysis Conference*, pages 1481–1487. Citeseer, 1999.

[63] M.L.M Duarte and D.J. Ewins. Some insights into the importance of rotational degrees-of-freedom and residual terms in coupled structure analysis. In *Proceedings-Spite The International Society for Optical Engineering*, pages 164–170. Leuven (Belgium), 1995.

[64] T. Gialamas, D. Tsahalis, L. Bregant, D. Otte, and H. Van der Auweraer. Substructuring by means of frfs: some investigations on the significance of rotational dofs. In *Proceedings-Spite the international society for optical engineering*, 619–625,1996.

[65] E.H. Bokelberg, H.J. Sommer III, and M.W. Trethewey. A six-degree-of-freedom laser vibrometer, part i: theoretical development. *Journal of sound and vibration*, 178(5):643–654, 1994.

[66] E.H. Bokelberg, H.J. Sommer III, and M.W. Trethewey. A six-degree-of-freedom laser vibrometer, part ii: Experimental validation. *Journal of Sound and Vibration*, 178(5):655 – 667, 1994.

[67] P. Avitabile and J. O'Callahan. Frequency response function expansion for unmeasured translation and rotation dofs for impedance modelling applications. *Mechanical Systems and Signal Processing*, 17(4):723 – 745, 2003.

[68] D. Montalvao, A.M.R. Ribeiro, N.M.M. Maia, and J.M.M. Silva. Estimation of the rotational terms of the dynamic response matrix. *Shock and Vibration*, 11(3-4):333–350, 2004.

[69] T.G. Carne and C.R. Dohrmann. Improving experimental frequency response function matrices for admittance modeling. In *Proceedings of the Nineteenth International Modal Analysis Conference*, 2006.

[70] P. Sjövall and T. Abrahamsson. Component system identification and state-space model synthesis. *Mechanical Systems and Signal Processing*, 21(7):2697–2714, 2007.

[71] L. Meirovitch. *Principles and techniques of vibrations*. Prentice Hall, Upper Saddle River, N.J, 1997.

[72] J. Bao and P.L. Lee. *Process Control: The Passive Systems Approach (Advances in Industrial Control)*. Springer Verlag London Limited, 1. aufl. edition, 2007.

[73] Y. Altintas. *Manufacturing Automation: Metal Cutting Mechanics, Machine Tool Vibrations and CNC Design*. Cambridge University Press, 2000.

[74] K. Weinert, T. Surmann, D. Enk, and O. Webber. The effect of runout on the milling tool vibration and surface quality. *Production Engineering*, 1:265–270, 2007.